储气库管柱冲蚀理论及预测研究进展

王志远，杨贺民，张洋洋，刘晓

（中国石油大学（华东）石油工程学院，山东 青岛 266580）

摘要：储气库的管柱冲蚀规律较复杂，且冲蚀预测难度较大，开展循环注采工况下的储气库管柱冲蚀理论、冲蚀预测方法研究具有必要性及迫切性。目前，针对储气库强采强注工况下的管柱冲蚀报道极少。综述了塑性材料及气主导体系管柱冲蚀机理、冲蚀预测方法，对保障储气库管柱注采安全具有一定借鉴意义。以塑性材料冲蚀机理为出发点，详细介绍了适用于管柱塑性材料的微切削、变形切削、挤压-薄片、局部变形、二次冲蚀及靶面热熔等六大典型冲蚀理论，并汇总其优缺点。指出适用于储气库管柱的冲蚀准则（材料的临界冲蚀流量、临界冲蚀流速、表面延展性、质量损失、体积损失、强度衰减）及冲蚀表征指标（冲蚀比、临界塑性应变、冲蚀损失率、材料剩余最小安全系数），针对这些指标介绍了目前国内外典型的旋转式、射流式、管流式、单颗粒冲蚀式实验系统，以及基于实验数据的冲蚀预测经验模型，如使用频率最高的 E/CRC 模型和 Oka 模型等。描述了基于 CFD 预测冲蚀的普遍流程及不足，分析了基于人工智能预测管柱冲蚀的可行性，这对保障储气库安全高效注采具有一定的理论指导及现实意义。

关键词：储气库管柱；冲蚀准则；冲蚀理论；冲蚀预测模型；冲蚀预测方法

中图分类号：TE983 **文献标识码：**A **文章编号：**1001-3660(2023)03-0091-20

DOI：10.16490/j.cnki.issn.1001-3660.2023.03.007

Research Progress on Erosion Theory and Prediction in Pipe String of Gas Storage

WANG Zhi-yuan, YANG He-min, ZHANG Yang-yang, LIU Xiao

(School of Petroleum Engineering, China University of Petroleum (East China), Shandong Qingdao 266580, China)

ABSTRACT: As natural gas develops to a specific scale in China, gas storage construction has become an inevitable tendency to realize the functions of natural gas peak regulation, emergency gas supply, and strategic reserve. Gas storage often owns a long operating life and adopts a multi-cycle fast and strong injection and extraction mode. Under the multi-cycle and high-intensity injection and extraction, the pipe string will inevitably suffer from the coupling effects of temperature, pressure and alternating cyclic load and will be exposed to an erosion risk. In addition, the gas storage is prone to fatigue damage and sand output under long-cycle alternating load, further aggravating the pipe string erosion. In conclusion, the erosion law of pipe string in gas storage is string and the erosion prediction is challenging, so it is necessary and urgent to study the erosion theory and the methods of erosion prediction for pipe string in gas storage under cyclic injection and extraction. At present, scholars

收稿日期：2022–02–27；**修订日期：**2022–05–19

Received：2022-02-27；**Revised：**2022-05-19

基金项目：广东省海洋经济发展（海洋六大产业）专项资金项目（粤自然资合[2021]56 号）

Fund：Guangdong Marine Economic Development (Six Marine Industries) Special Fund Project（GDNRC[2021]56）

作者简介：王志远（1981—），男，博士，教授，主要研究方向为油气井多相流动理论及应用。

Biography：WANG Zhi-yuan (1981-), Male, Doctor, Professor, Research focus: theory and application of multiphase flow in oil and gas wells.

引文格式：王志远，杨贺民，张洋洋，等. 储气库管柱冲蚀理论及预测研究进展[J]. 表面技术, 2023, 52(3): 91-110.

WANG Zhi-yuan, YANG He-min, ZHANG Yang-yang, et al. Research Progress on Erosion Theory and Prediction in Pipe String of Gas Storage[J]. Surface Technology, 2023, 52(3): 91-110.

from China and abroad have conducted much research on the erosion of plastic material and have achieved many results. However, these results mainly analyze plastic material erosion in gathering pipelines and specific working conditions, and few reports are available for the pipe string erosion in gas storage under the robust extraction and injection. Therefore, reviews on the erosion mechanism for plastic materials and pipe string in the gas-dominated system and erosion prediction are of specific significance to ensure the safety of pipe string in gas storage during gas injection and extraction.

With erosion mechanism as the focus, six typical corrosion theories suitable for plastic materials of pipe string, such as micro-cutting, deformation-cutting, forging extrusion, local deformation, secondary corrosion and hot melt on the target surface were described, and the advantages, disadvantages, and application scope of each theory were clarified. The corrosion criteria (critical erosion flow volume and critical erosion flow rate, surface ductility, mass and volume loss, and strength decay) and the erosion indexes (flow rate ratio, critical plastic strain, a loss rate of mass and volume, and the remaining minimum safety factor) applicable to the pipe string in gas storage were summarized. The specific calculation methods of the indexes were also given. Typical experimental systems from China and abroad were introduced, such as rotating, jet, tubular flow, and single-particle erosion. Several empirical erosion models based on the experimental data, like the E/CRC model and Oka model with a higher frequency of utilization, were given. However, the related standards or specifications for erosion experiments have not been developed in China and abroad, so the erosion law of pipe string has not been systematically studied. The unified interpretation of experimental phenomena and erosion mechanisms under different working conditions and the establishment of universal models for erosion prediction have not been realized. Given the suitable selection of erosion models being a priori existence, this limitation becomes the key to improving the erosion prediction accuracy when using CFD. The general process and shortcomings of predicting erosion based on CFD are described, and the feasibility of predicting pipe erosion based on artificial intelligence is analyzed, which has certain theoretical guidance and practical significance for ensuring safe and efficient injection and production of gas storage. The erosion prediction methods based on artificial intelligence can improve the prediction accuracy of erosion rates. However, the method is in the initial exploration stage and is subject to many limitations in selecting machine learning algorithms and their application settings, requiring much experimental validation.

KEY WORDS: pipe string of gas storage; erosion criteria; erosion theory; erosion prediction model; erosion prediction method

目前，国内天然气田分布与需求极不匹配，跨季度天然气需求差异大，供需矛盾愈发突出。为了实现天然气的调峰保供、应急供气、战略储备等功能，储气库成为我国天然气发展到一定规模时的必然需求。中国科学院院士邹才能认为储气库建设在一定程度上是一项政治工程、民生工程和保障工程[1]。特别是“十四五”期间，在“加强天然气供销体系”“实现碳达峰、碳中和”的宏观能源目标驱动下，我国储气库建设步伐逐渐加快[2-4]。我国储气库以油气藏型为主（占比达到 76%以上），不同于油气藏的稳产追求，储气库往往采用多周期快注快采、强注强采的运营模式，且运行年限通常要求为 30~50 年[5]。明显地，在多周期高强度循环注采下，储气库管柱将不可避免地会遭受温度、压力、交变循环载荷等耦合作用，存在管柱冲蚀风险，如图 1 所示[6]。管柱冲蚀发生后的直接结果是导致管柱壁厚变薄、强度衰减，最终限制储气库的注采能力，这对管柱的完整性提出了巨大挑战。此外，在长周期交变载荷下储层易发生疲劳损伤，出砂风险较高，会进一步加剧管柱冲蚀，使得管柱安全运行管理难度增大[7-9]。陆地与海上储气库管柱冲蚀特征对比如表 1[10-14]所示，可见开展交替注采工况下陆地和海上储气库管柱冲蚀预测研究具有迫切性和必要性。

冲蚀是流体及流体携带相（如液滴、砂粒、岩屑等颗粒）以一定角度、速度撞击材料表面（靶面）并导致靶面变形及材料损失的一种现象。储气库管柱多为塑性材料（如 N80、P110、S13Cr、M13Cr、13Cr、SM80S 等[15]），且管柱冲蚀通常存在较长的孕育期，即靶面被颗粒冲击后不会立即产生冲蚀，而是首先变得粗糙，并发生表面硬化现象。此时靶面存在损伤，但未出现质量损失，仅当损伤积累到一定程度时靶面才会出现冲蚀。迄今为止，针对塑性材料冲蚀磨损，

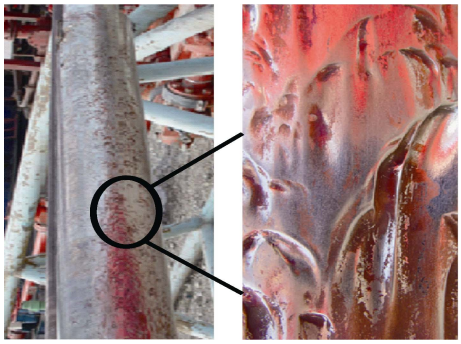

图 1 管柱安全阀冲蚀的宏观及微观形貌[6]

Fig.1 Macro and micro erosion morphologies of pipe string safety valve[6]

表 1　陆地与海上储气库管柱冲蚀特征对比[10−14]

Tab.1 Comparison of pipe string erosion characteristics between onshore and offshore gas storages[10-14]

Gas storage type	Same characteristics	Different characteristics
Onshore Offshore	Multi cycle strong injection and production, long service time of pipe string, prediction and protection of pipe string erosion are difficult	The gradient of temperature and pressure field of injection and production wells in offshore gas storage is greater than that in onshore gas storage, with less quantity, stronger requirements for injection and production capacity of single well and higher risk of reservoir sand production, resulting in more complex law of pipe string erosion

国内外学者进行了大量研究，并取得了诸多成果。这些成果大多针对集输管道及特定工况下塑性材料的冲蚀分析，关于陆地或海上储气库注采管柱冲蚀的研究报道较少。本质原因在于储气库管柱具有造斜、变径、注采强度高、寿命周期要求长、固相砂粒运动轨迹多变、轨迹追踪难度大等特征。当管柱存在积液时，砂粒与液滴、液膜间的相互作用将不可忽略，这给颗粒撞击速度及管柱冲蚀程度的预测带来极大的挑战[16-18]。此外，即使抛开储气库管柱现场注采条件，目前在塑性材料冲蚀机理、多参数下的靶面冲蚀规律、冲蚀预测模型适用性及应用效果等方面仍存在一定争论[19-20]。鉴于此，文中基于塑性材料经典冲蚀理论，概述了管柱冲蚀准则和表征指标，介绍了目前国内外典型的冲蚀实验系统及基于实验数据的冲蚀预测经验模型，针对经验模型的不足，分析了基于计算流体力学（CFD）及人工智能预测管柱冲蚀的可行性，这对储气库的安全高效注采具有一定的理论指导及现实意义。

1　管柱冲蚀准则及表征指标

针对固相颗粒反复撞击储气库管柱靶面引发的冲蚀问题，引入某种准则来辨识或预测具体工况下靶面是否发生冲蚀及冲蚀严重程度是极有必要的。基于这两大工程需求，已衍生出通过材料的临界冲蚀流量、临界冲蚀流速、表面延展性、质量损失、体积损失、强度衰减等相关参数作为管柱靶材的冲蚀评价准则，如图 2 所示。这些冲蚀准则分别对应某一时空下的冲蚀比 v_r、临界塑性应变 ε_c、冲蚀损失率 $\overline{E}$、管柱剩余最小安全系数 S_e 等材料冲蚀表征指标。

目前存在诸多经验模型（如 API RP 14E 方程[21-22]、Beggs 方程[23]、Salama 方程[24]等，其优缺点见表 2），可对临界冲蚀流速和冲蚀流量进行估算，如式（1）—（3）所示。通过对比管柱内流体实际流速 v 与临界冲蚀流速 v_e 可判定靶面是否发生冲蚀失效。进一步地，可将 v 与 v_e 的比值定义为冲蚀流速比（简称冲蚀比 v_r），见式（4）。当 v_r 小于 1 时，材料不会发生冲蚀失效，无需采用防冲蚀手段；反之，材料存在较高概率发生冲蚀失效，需采取相应解决措施。

冲蚀涉及靶面塑性变形的累积，表现为冲击薄片的形成及冲击薄片的去除，仅当撞击区域的塑性变形累积至一定程度时（撞击颗粒数量大于冲蚀孕育所需数量），该区域才会发生冲击薄片的去除，并导致稳定冲蚀，且产生稳定冲蚀前的塑性变形累积量受到靶面延展性的影响[25-27]。基于此，临界塑性应变 ε_c 的概念被引入，以衡量靶面延展性，并作为靶面是否发生冲蚀的表征指标之一，见式（5）[28-29]。当靶面塑性应变 ε 达到 ε_c 时，靶面将发生稳定冲蚀，且 ε_c 越高表示靶材的延展性越好，越不容易发生冲蚀。

$$v_e = \frac{C}{\sqrt{\rho_m}} \tag{1}$$

$$v_e = \frac{SD_w\sqrt{\rho_m}}{\sqrt{W}} \tag{2}$$

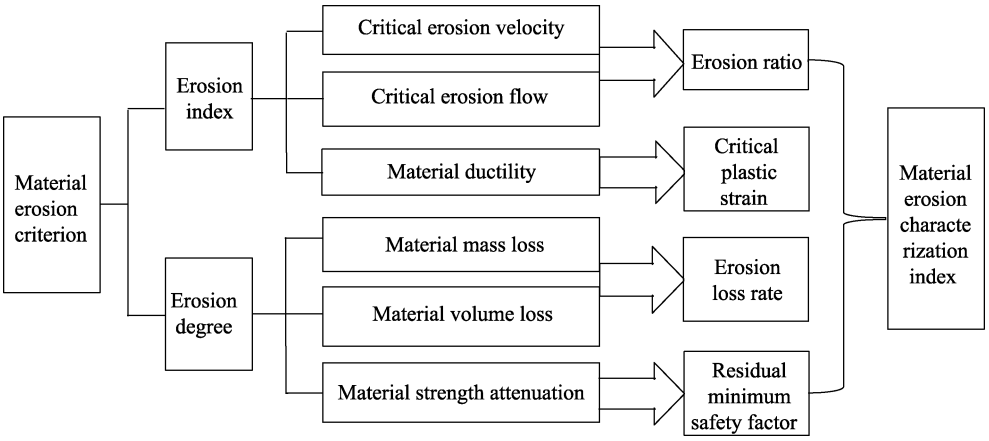

图 2　管柱材料冲蚀准则与表征指标的对应关系

Fig.2 Corresponding relationship between erosion criterion and characterization index of pipe string material

表 2 3 种常见管柱冲蚀预测模型对比[21−24]

Tab.2 Comparison of three common pipe string erosion prediction models[21-24]

Model	Formula	Considerations	Advantages and disadvantages	Scope of application
API RP 14E	$v_e=\frac{C}{\sqrt{\rho_m}}$	Fluid density, Empirical parameters	Without considering sand production and string friction, the calculation is simple, but the result is relatively conservative. The key prediction of empirical parameter C needs to rely on a large amount of field data	It is suitable for gas well string without sand or low water cut and production string of gas storage
Beggs	$q_e=3.33\times10^{-4}CD_w^2(p/ZT\gamma_g)^{0.5}$	Temperature, Pressure, Compressibility factor Relative fluid density, Empirical parameters		
Salama	$v_e=\frac{SD_w\sqrt{\rho_m}}{\sqrt{W}}$	Temperature, Pressure, Fluid density, Sand production, String shape	Considering more factors, the calculation results are more consistent with the on-site production conditions	It is mainly applicable to the erosion prediction of gas-liquid two-phase flow elbow with sand, which has been used in relevant gas well production sites abroad

$$q_e=3.33\times10^{-4}CD_w^2(p/ZT\gamma_g)^{0.5} \tag{3}$$

$$v_r=\frac{v_{(P,T)}}{v_e} \tag{4}$$

$$\varepsilon_c=\Delta\varepsilon_e N_f^{1/2} \tag{5}$$

式中：v_e 为颗粒临界冲蚀流速，m/s；C 为经验冲蚀系数，由靶材的属性决定；ρ_m 为含颗粒流体的密度，kg/m^3；S 为管柱形状系数，S 为 0~1；W 为单位时间的出砂量，kg；q_e 为临界冲蚀流量，m^3/d；D_w 为管柱直径，mm；P 为冲蚀流体压力，MPa；Z 为管柱流体压缩因子；T 为靶面撞击区域温度，K；γ_g 为流体相对密度，无量纲；$v_{(P,T)}$为含颗粒流体的速度，m/s；ε 为靶面塑性应变；$\Delta\varepsilon_e$为单个颗粒撞击引发的靶面塑性应变增量；N_f为靶面材料去除所需要的颗粒平均撞击次数。

靶材损失本质为质量损失，$\overline{E}$ 主要通过单位时间的冲蚀靶面质量损失 $\Delta\overline{E}_m$、靶面体积损失 $\Delta\overline{E}_v$、靶面厚度损失 $\Delta\overline{E}_l$，或冲蚀率 E_R 等指标进行表征。其中，$\Delta\overline{E}_m$ 可由 DNV 标准（式 6）粗略表示[30]，E_R 为颗粒速度、攻角、靶面硬度、靶材密度、颗粒粒径、颗粒密度、颗粒硬度及颗粒锐度等因素的复合函数，见式（7）；$\Delta\overline{E}_l$ 可由 $\Delta\overline{E}_m$ 换算得出，见式（8）。

美国石油协会（API）规定 $\Delta\overline{E}_l$ 的阈值为 0.076 mm/a[31]，若管柱壁面冲蚀速率不超过 0.076 mm/a，可认为管柱所受冲蚀在可接受范围内，此时管柱不会发生冲蚀失效。需注意，基于计算流体力学（CFD）开展靶材冲蚀预测时，靶面冲蚀速率的单位分别为 kg/(m^2·s)（稳态法）、kg/m^2（瞬态法）。管柱剩余最小安全系数 S_e 本质上在于对冲蚀后管柱剩余抗内压强度、剩余抗拉强度及剩余抗挤强度的计算，可由 $\Delta\overline{E}_l$ 进行估算，见式（9）。

$$\Delta\dot{E}_m=\dot{m}_p\times C\times v_p^n\times F(\alpha) \tag{6}$$

$$E_R=\frac{E_m}{E_p}=f(v_p,\alpha,H_t,\rho_t,\rho_p,d_p,F_s) \tag{7}$$

$$\Delta\dot{E}_l=\frac{\Delta\dot{E}_m\times24\times365\,000}{\gamma\times n^*\times A_t} \tag{8}$$

$$S_e^n=\frac{L_0-\Delta\dot{E}_l\times n^*}{L_0}\times S_0 \tag{9}$$

式中：$\Delta\dot{E}_m$ 为单位时间的靶面质量损失，kg/a；E_m 为靶面质量损失，kg；$\Delta\overline{E}_l$ 为单位时间的靶面厚度损失，mm/a；E_p 为撞击颗粒的质量，kg；E_R 为冲蚀率，即颗粒质量与靶面质量损失的比值；$\overline{m}_p$ 为撞击颗粒的质量流量，kg/s；n 为冲蚀经验系数，n 为速度指数，由靶材属性决定，具体取值如表 3 所示[30]；v_p 为颗粒速度，m/s；α 为攻角，(°)；H_t 为靶面硬度，HB；ρ_t 为靶材密度，kg/m^3；ρ_p 为固体颗粒密度，kg/m^3；d_p 为固相颗粒粒径，mm；F_s 为颗粒形状系数，F_s 为 0~1；$F(\alpha)$为攻角函数，表征材料的延展性，可由式(10)计算[32]；C_i(i=1, 2, 3,…, 8)为常数，具体取值如表 4 所示；γ 为冲蚀样品容重，N/m^3；A_t 为冲蚀靶面面积，m^2；S_e^n 为 n 年后的靶材剩余安全系数；n^*为冲蚀持续时间，a；L_0 为靶材原始厚度，mm；S_0 为靶材初始安全系数。

$$F(\alpha)=\sum(-1)^{(i+1)}C_i\left(\frac{\alpha\times\pi}{180}\right)^i \tag{10}$$

表 3 K、n 的取值[30]

Tab.3 K, n values[30]

Material	Material density/(kg·m^{-3})	K/[(m·s^{-1})$^{-n}$]	n
Steel	7 800	2.0	2.6
Titanium	4 500		
Fiberglass/Epoxy resin	1 800	0.3	3.6
Fiberglass/Vinyl ester		0.6	

表 4　C_i的取值[30,32]

Tab.4 C_i value[30,32]

C_1	C_2	C_3	C_4	C_5	C_6	C_7	C_8
9.370	42.295	110.864	175.804	170.137	98.398	31.211	4.170

2　塑性材料冲蚀机理

储气库管柱以塑性材料为主，因此塑性材料冲蚀机理是预测管柱冲蚀的基础。冲蚀理论多基于观察靶面冲蚀微观形貌建立，实验依赖性较强，但仍是不同工况下冲蚀微观形貌向宏观预测模型转化的必要手段。塑性材料冲蚀理论主要包括微切削、变形切削、挤压−薄片剥落、局部变形、二次冲蚀、靶面热熔等，这些理论的关注点不尽相同，具有适用于特定工况的共同特征。

2.1　微切削理论

微切削理论是世界上首个描述塑性材料冲蚀机理的理论。该理论由 Finnie[33-35]提出，他认为大量固体磨粒以一定角度高速撞击靶面时，磨粒的尖角类似于微型刀具，会直接刺入材料表面，并将靶面材料以切削方式带走，机理如图 3 所示[36]。Budinskif[37]通过室内冲蚀实验将这种微切削现象进一步细分为点削、犁削、铲削和切削，之后 Alam 等[38]通过冲蚀实验证实了犁削及切削现象，如图 4 所示。基于切削原理，该理论较完整地表达了冲蚀体积损失量与磨粒质量、颗粒冲蚀角度、颗粒撞击速度的定量关系，见式(11)。单个颗粒冲蚀 3 种不同塑性材料时，冲蚀体积相对损失量随冲蚀角度变化的实验值和理论计算值对比如图 5 所示。由图 5 可知[35]，微切削理论能够准确预测低冲蚀角度下（15°~20°）的靶材冲蚀程度。当冲蚀角度较大时，该理论计算值与实际值的误差较大。当冲击角度达到 90°时，该理论的计算值为 0，这与实际冲蚀情况严重不符。当颗粒冲蚀角度为 15°~20°时，冲蚀体积损失量可近似由式（12）表示，即冲蚀体积损失量估计为 7.5%的粒子动能除以流体压力。

Hashish[39]考虑了颗粒圆球度，并调整了速度指数，进一步优化了 Finnie 模型，见式（13）。该优化模型仍在较小攻角下才具有较高的冲蚀预测精度，能较好地解释塑性材料在多角形磨粒、小冲蚀角下的材料冲蚀规律，但不适用于大攻角的冲蚀预测。受到颗粒速度指数的影响，颗粒速度对冲蚀的准确作用关系也较难表征。

$$E_v=\begin{cases}\dfrac{m_p v_p^2}{8p}(\sin 2\alpha-3\sin^2\alpha) & \alpha\leqslant 18.5^\circ\\ \dfrac{m_p v_p^2}{24p}\cos^2\alpha & \alpha>18.5^\circ\end{cases} \tag{11}$$

$$E_v\approx 0.075\frac{m_p v_p^2}{2p} \tag{12}$$

$$E_v\approx\frac{7}{\pi}\frac{m_p}{\rho_p}\left(\frac{v_p}{C_k}\right)^{2.5}\sin 2\alpha(\sin\alpha)^{1/2} \tag{13}$$

式中：E_v 为颗粒撞击引起的冲蚀体积损失量，m^3；m_p 为单颗颗粒质量，kg；v_p 为颗粒速度，m/s；σ_y 为弹性载荷极限，kN/m^2；C_k 为经验系数，由式（14）计算。

$$C_k=\sqrt{\frac{3\sigma_y F_s^{3/5}}{\rho_p}} \tag{14}$$

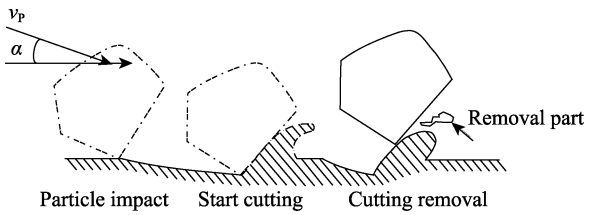

图 3　颗粒冲蚀过程中的切削示意图

Fig.3 Schematic diagram of cutting during particle erosion

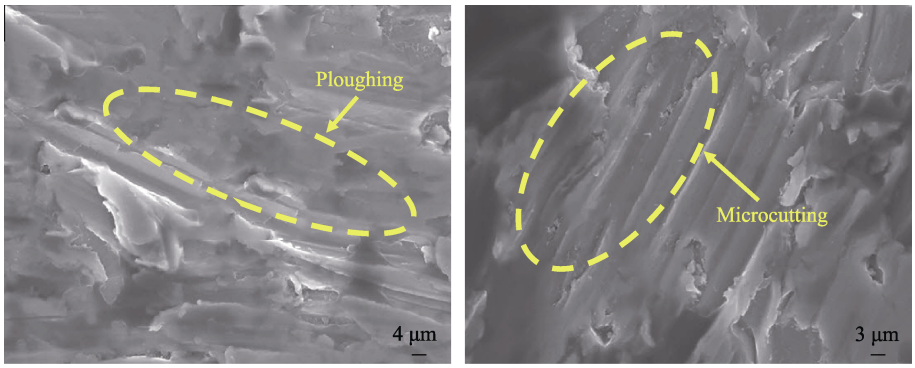

a 靶面在颗粒犁削冲蚀作用下的微观形貌　　b 靶面在颗粒切削冲蚀作用下的微观形貌

图 4　颗粒冲蚀过程中的犁削和切削实测图[38]

Fig.4 Measurement of ploughing and microcutting in particle erosion process[38]: a) micro morphology of target surface under the action of ploughing particles; b) micro morphology of target surface under the action of microcutting particles

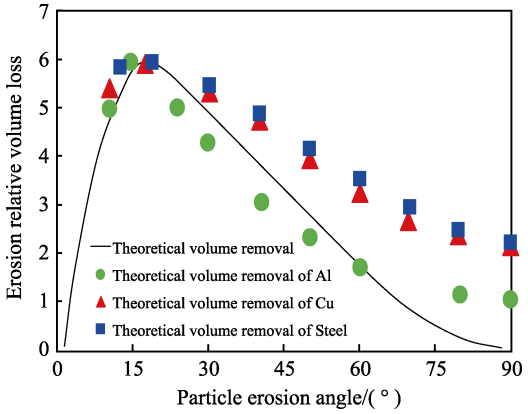

图 5　Finnie 理论中冲蚀体积相对损失量随冲蚀角度的变化情况[35]

Fig.5 Variation of relative loss of Finnie theoretical erosion volume with erosion angle[35]

2.2　变形切削理论

颗粒冲击速度可分解为垂直于靶面的法向分量和与靶面相切的切向分量，前者使靶面产生变形损伤，后者使靶面材料发生切削和去除（图 6）[40]。基于此，Bitter[41-42]认为，当磨粒的冲击应力低于靶面屈服强度（颗粒法向速度小于发生塑性应变的临界速度）时，靶面材料仅发生弹性变形（仅产生颗粒的碰撞回弹，不发生冲蚀磨损），反之则发生弹性和塑性 2 种变形。此时输入颗粒动能将转化为颗粒回弹动能和靶面塑性应变能，后者是形成变形磨损、切削磨损的基础，通常变形磨损与切削磨损的比值随着攻角的增大而逐渐增大。诸多学者将回弹速度 v_r 与颗粒速度 v_p 的比值定义为恢复系数 e，该值代表靶面储存弹性变形能的能力，e 越大，说明靶面储存的弹性变形能越多，即靶面产生的塑性变形较少，变形磨损与切削磨损程度较低[43]。此外，颗粒对靶面的反复冲击还会使材料产生表面硬化，提高靶面的弹性极限或发生塑性应变的临界速度，变形磨损占比会进一步增大[44]。

基于磨粒冲入、挤出靶材过程的能量平衡，变形磨损量、切削磨损量及总冲蚀磨损量可表示为式（15）—（17）[41-42]。Neilson 等[45]针对大攻角下部分颗粒会停留在靶面的现象，简化了 Bitter 模型，简化模型如式（18）所示。Huang 等[40]基于变形切削理论推导出靶面压痕体积方程，采用临界塑性应变及 Coffin−Manson 方程计算了变形损伤去除量，并在靶面实际切削量与切削体积成正比、与靶材延展性成反比的假设下，得到了变形损伤去除和切削去除组合的总体积损失，见式（19）。相较于微切削理论，该理论同时考虑了材料冲击后的弹性变形和塑性变形，因此针对高、低攻角下塑性材料的冲蚀情况均具有较好的预测精度。该理论已被诸多学者通过观察撞击靶面的压痕形貌所证实[46-47]。不过，该理论具有不可忽略的 η、ε、C、K_1、D 等经验参数，这些参数必须通过冲蚀物理实验来获取，因此该模型不能直接预测出靶面冲蚀结果，这在一定程度上限制了该理论的拓展[48-49]。

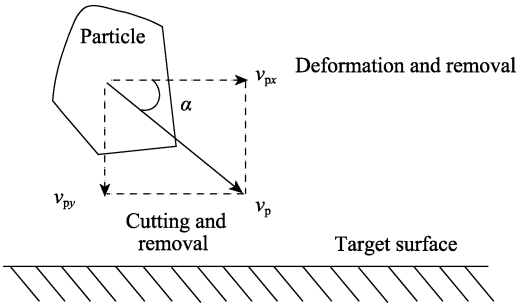

图 6　颗粒撞击靶面时的法向分量和切向分量

Fig.6 Normal and tangential components of particles impacting the target surface

$$E_{vc}=\begin{cases}\dfrac{2m_pC_1(v_p\sin\alpha-v_e)}{(v_p\sin\alpha)^{1/2}}\left[v_p\cos\alpha-\dfrac{C_1(v_p\sin\alpha-v_e)^2}{(v_p\sin\alpha)^{1/2}}\eta\right] & \alpha\leqslant\alpha_0\\ \dfrac{m_pC_1}{2\eta}[v_p^2\cos^2\alpha-K_1(v_p\sin\alpha-v_e)^{3/2}] & \alpha>\alpha_0\end{cases}\tag{15}$$

$$E_{vd}=\begin{cases}0 & v_p\sin\alpha\leqslant v_e\\ \dfrac{m_p(v_p\sin\alpha-v_e)^2}{2\Phi} & v_p\sin\alpha\geqslant v_e\end{cases}\tag{16}$$

$$E_v=E_{vc}+E_{vd}\tag{17}$$

$$W=\begin{cases}\dfrac{2m_pv_p^2\cos^2\alpha}{2\eta}+\dfrac{m_p(v_p\sin\alpha-v_e)^2}{2\Phi} & \alpha\geqslant\alpha_0\\ \dfrac{2m_pv_p^2\cos^2\alpha\sin\alpha}{2\eta}+\dfrac{m_p(v_p\sin\alpha-v_e)^2}{2\Phi} & \alpha<\alpha_0\end{cases}\tag{18}$$

$$E_R\approx D\rho_p^{0.1875}d_p^{0.5}v_p^{2.375}\cos^2\alpha\sin^{0.375}\alpha\tag{19}$$

式中：E_{vc} 为切削磨损引起的单位体积损失量，m^3；E_{vd} 为变形磨损引起的单位体积损失量，m^3；α_0 为颗粒临界攻角，(°)，塑性材料的临界攻角约为 20°；v_e 为颗粒临界冲蚀速度，m/s，由式（20）计算；η、Φ 分别为切削磨损系数和变形磨损系数，均由实验确定；μ_p、μ_t 分别为颗粒和靶材的泊松比；E_1、E_t 分别为颗粒和靶材的弹性模量，MPa；C_1、K_1 为经验系数，分别由式（21）、（22）计算；D 为与靶材相关的经验系数。

$$v_e=\frac{1.54\sigma_y^{5/2}}{\rho_p^{1/2}}\left[\frac{1-\mu_p^2}{E_1}+\frac{1-\mu_t^2}{E_t}\right]\tag{20}$$

$$C_1=\frac{0.288}{\sigma_y}\sqrt[4]{\frac{\rho_p}{\sigma_y}}\tag{21}$$

$$K_1=0.82\sigma_y^2\sqrt[4]{\frac{\sigma_y}{\rho_p}}\left[\frac{1-\mu_p^2}{E_1}+\frac{1-\mu_t^2}{E_t}\right]\tag{22}$$

2.3　挤压–薄片剥落理论

挤压–薄片剥落理论又称锻造–挤压理论，具体的挤压锻造过程如图 7 所示。Rickerby 等[27]和 Levy[50-51]通过 SEM 观察大量靶材冲蚀微观形貌（图 8a）后发现，单颗粒撞击靶面后冲蚀坑（图 8b）会挤出，并堆积大量软化畸形薄片（图 8c），认为这些畸形薄片由挤压锻造作用所致。换言之，颗粒冲击靶面可视为颗粒对靶面的挤压锻造，反复地挤压锻造会使靶面产生严重的塑性变形及较高的靶面温度。当靶面温度接近材料的退火温度时，软化畸形薄片开始出现，并逐渐剥落（薄片的延展性破裂）。畸形薄片的锻打还会在靶材软化层下产生表面硬化层（见图 8d），该层相较于靶面的质地更为坚硬（图 8e、f），能有效促进表面软化层的剥落[44,52]。通过实验还发现，一定数量的颗粒在冲蚀发生前就已撞向靶面，且靶面的初始质量损失低于一段时间后的质量损失，证实靶面稳定冲蚀存在一定的孕育过程。当表面硬化层达到稳定硬度和厚度时，稳态冲蚀才开始，且冲蚀速率取决于表面硬

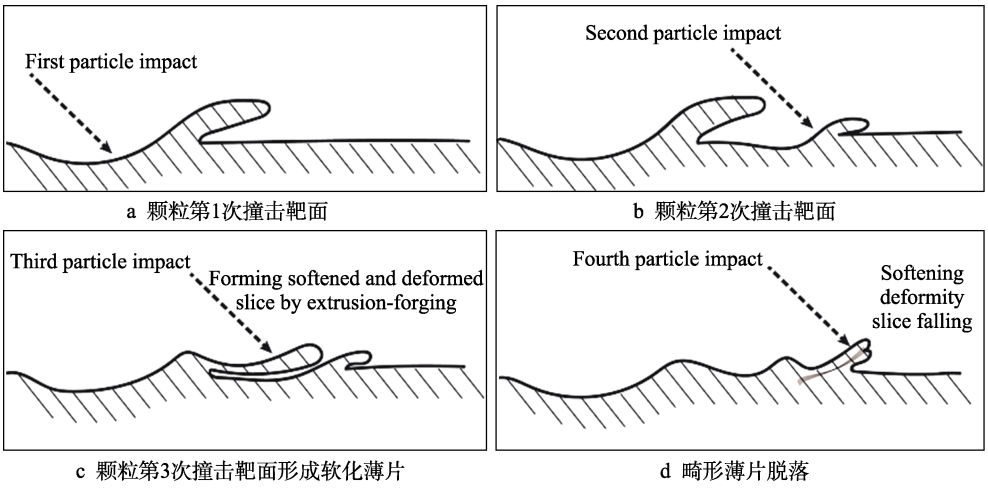

a 颗粒第1次撞击靶面　　b 颗粒第2次撞击靶面

c 颗粒第3次撞击靶面形成软化薄片　　d 畸形薄片脱落

图 7　靶面材料的挤压锻造过程示意图

Fig.7 Schematic diagram of extrusion forging process of target surface material: a) the first impact of particles on the target surface; b) the second impact of particles on the target surface; c) the third impact of particles on the target surface to form a softened and deformed sheet; d) falling of the softened deformity slice

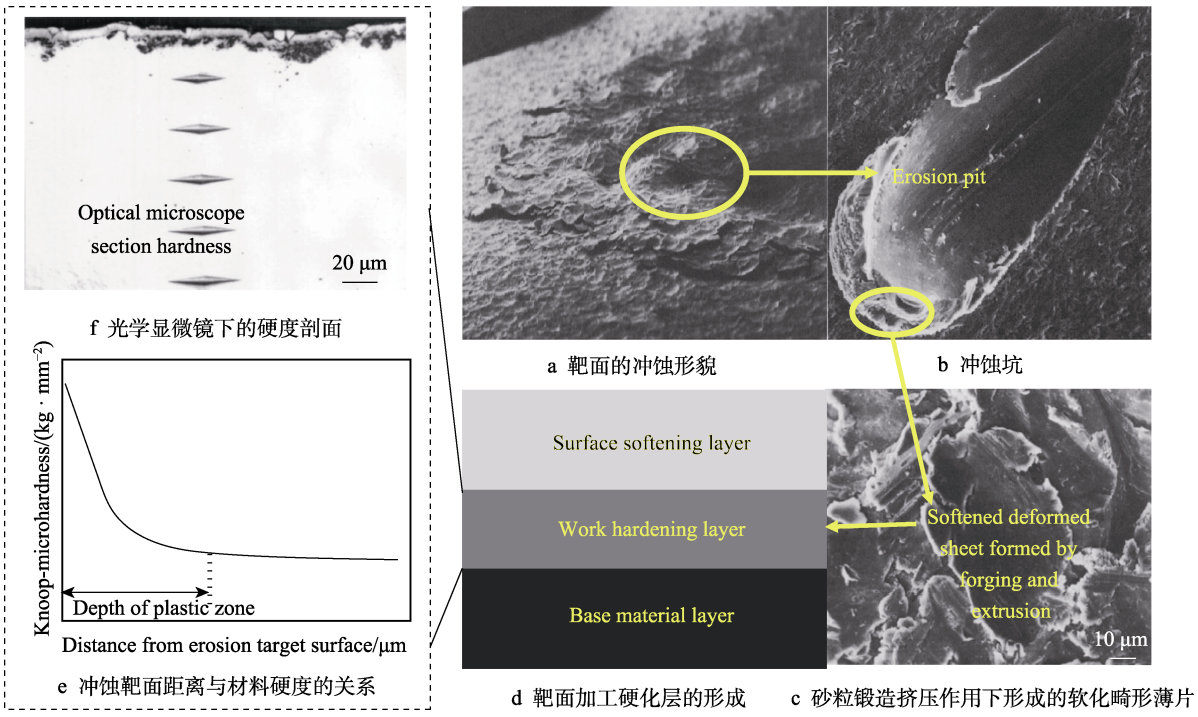

f 光学显微镜下的硬度剖面

e 冲蚀靶面距离与材料硬度的关系

a 靶面的冲蚀形貌　　b 冲蚀坑

d 靶面加工硬化层的形成　　c 砂粒锻造挤压作用下形成的软化畸形薄片

图 8　靶面材料的挤压锻造实测图[27,44,50-52]

Fig.8 Actual measurement for extrusion forging of target surface material[27,44,50-52]: a) surface morphology of target; b) erosion pits; c) softened and deformed sheet formed on target surface due to forging and extrusion of sand particles; d) formation of work-hardened layer on target surface; e) relationship between the distance of erosion target and the material hardness; f) profile hardness based on the optical microscope

化层的性质，这解释了微切削理论难以说明的滞后冲蚀现象[27]。锻造−挤压理论能有效解释颗粒冲蚀下塑性材料的冲蚀形貌和冲蚀规律，但该理论迄今并未量化出相应的理论预测模型，因此常用于塑性材料冲蚀的定性分析。

2.4　局部变形理论

基于颗粒撞击靶面引起的塑性变形累积，Hutchings 等[28]选用靶面硬度和延展性 2 个物理量来描述靶面的抗冲蚀性能，并采用临界塑性应变 ε_c 准则来判断颗粒撞击时靶面是否发生冲蚀，即颗粒撞击挤压造成的唇片变形量达到 ε_c 后，靶面上因冲蚀造成的唇片开始剥离。基于该准则建立的冲蚀模型如式（23）所示，材料的冲蚀机制并未详细说明。此外需注意，ε_c 并非为常数，它受到唇片应变速率和靶面温度的双重影响。Sundararajan 等[53-54]将撞击区域热效应激发的材料局部流动定义为变形局部化，并指出 ε_c 是变形局部化的体现。基于此，Christman 等[55]把靶面冲蚀分为 3 个过程：撞击区域发生绝热变形；撞击区域局部化变形，形成绝热剪切带；绝热剪切带演化为变形唇片，并以磨屑形式脱落。这一冲蚀理论也被邵荷生等[56]所证实（见图 9）。变形局部化冲蚀模型可由式（24）表示，该模型考虑了靶材热物理性质对冲蚀速率的影响，之后 Sundrarajan 综合考虑了变形局部化与靶面能量吸收的关系，进一步优化了该模型，见式（25）。由于变形局部化的临界条件在本质上是剪切应变局部化的条件，因此该模型仅适用于易受绝热剪切破坏的靶材。Chen 等[57]在假设残余拉应力是变形唇片脱落主要原因的基础上，应用 Johnson−Cook 断裂模型，推导了 E_R 预测模型，见式（26），确定了靶材去除体积与撞击压痕体积的比值。该模型可以很好地评估应变速率和温升对冲蚀速率的影响。通过计算发现，相较于靶材应变硬化和热效应激发，靶材几何性质对变形唇片的形成具有显著影响。

$$E_R = 0.033\frac{C\rho_t\rho_p^{1/2}v_p^3}{\varepsilon_c^2 H_t^{3/2}} \tag{23}$$

$$E_R = 6.5\times10^{-3}\frac{\rho_p^{1/4}v_p^{2.5}}{C_t T_{melt}^{3/4} H_t^{1/4}} \tag{24}$$

$$E_R = (2^{n_h} C v_p^2 \sin^2\alpha F(t)/n_h C_t)\cdot \left\{1+\left[(n_h+1)\frac{\varphi(e)}{\varphi_{max}(e)}\left(2-\frac{\varphi(e)}{\varphi_{max}(e)}\right)\Big/4(1+\lambda)\tan^2\alpha F(t)\right]-e^2\right\} \tag{25}$$

$$E_R = \frac{0.064\rho_t\rho_p^{0.5}v_p^3}{(D_1+D_2\exp D_3\sigma^*)^2(1+D_4\ln\varepsilon^*)^2(1+D_5T^*)^2 p^{-3/2}} \tag{26}$$

式中：T_{melt} 为靶面热熔温度，K；C_t 为靶材比热容，J/(kg·℃)；n_h 为靶面的应变硬化系数；e 为恢复系数，可分为法向恢复系数 e_n 和切向恢复系数 e_t；$\varphi(e)$为靶面的临界摩擦因数，是关于 e 的一个函数；$\varphi_{max}(e)$为靶面临界摩擦因数最大值；$F(t)$为常数，用来表达颗粒多次撞击靶面同一位置时塑性应变的累积及塑性应变梯度的形成过程；$\lambda=r^2/k^2$，r 为颗粒质心与靶面间的距离（mm），对于球形颗粒，$r=d_p$，k 为颗粒回转半径（mm）；σ^*为冲蚀流体压力与靶面应力之比，$\sigma^*=P/\sigma$；ε^*为靶面塑性应变与 ε 与临界塑性应变 ε_c 之比；$T^*=(T-T_{en})/(T_{melt}-T_{en})$，$T_{en}$ 为环境温度（K）；D_1、D_2、D_3、D_4、D_5 为经验常数。

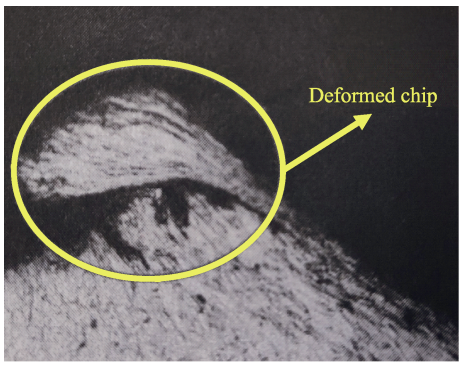

图 9　绝热剪切带演化形成典型的变形唇片[56]
Fig.9 Evolution of adiabatic shear zone to form typical deformed chip[56]

2.5　二次冲蚀理论

以上讨论的冲蚀理论通常将撞击颗粒看作不发生断裂的刚体，事实上颗粒冲击靶面后会发生一定程度的破碎，这些破碎部分可能会对靶面产生二次冲蚀破坏。基于此，Tilly[58]利用高速摄像机、电子显微镜等微观测手段研究了颗粒破裂对塑性材料冲蚀的影响。通过测量冲击前后颗粒的尺寸发现，粒径与冲击速度较小的颗粒基本不发生破碎，此时只造成一次冲蚀，仅当颗粒尺寸及冲击速度达到某临界值时，颗粒才会发生破碎，并造成二次冲蚀，如图 10 所示。由此可见，塑性材料冲蚀可分为以下 2 个阶段：颗粒撞击靶面产生压痕，压痕周围被挤压或去除的材料形成

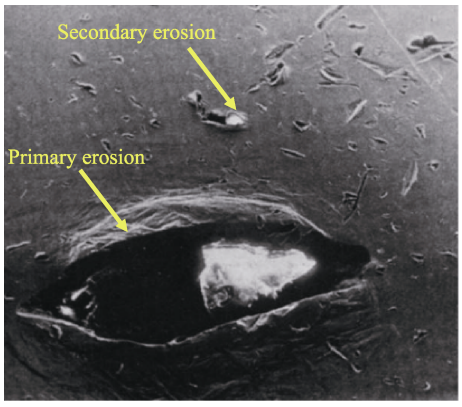

图 10　靶面材料的一次冲蚀及二次冲蚀示意图[58]
Fig.10 Schematic diagram of primary and secondary erosion of target surface[58]

脆弱的小丘；颗粒在撞击靶面时破碎，然后碎片呈放射状向周围投射，并产生二次冲蚀破坏。其中，一次冲蚀、二次冲蚀及总冲蚀磨损量可由式（27）—（29）表示。此外，Tilly 实验还证实在低攻角下二次冲蚀的占比较小，在较高攻角下二次冲蚀的占比提高，但该理论并未完全解释在高攻角下的靶面材料损失机制。

$$E_{v1}=E_{v1_{max}}\left(\frac{v_p}{v_k}\right)\left[1-\left(\frac{d_{p0}}{d_p}\right)^{3/2}\left(\frac{v_e}{v_p}\right)\right]^2 \tag{27}$$

$$E_{v2}=E_{v2_{max}}\left(\frac{v_p}{v_k}\right)^2 f \tag{28}$$

$$E_v=E_{v1}+E_{v2} \tag{29}$$

式中：E_{v1} 为单位颗粒质量的一次冲蚀去除量，m^3；E_{v1max} 为一次冲蚀的极限去除量，m^3；E_{v2} 为单位颗粒质量的二次冲蚀去除量，m^3；E_{v2max} 为二次冲蚀极限去除量，m^3；v_k 为一次冲蚀极限去除量对应的颗粒速度，m/s；d_{p0} 为固相颗粒临界冲蚀粒径，mm；f 为颗粒破碎程度，与颗粒冲击速度、颗粒尺寸及攻角密切相关，可由式（30）计算；m_0 为冲蚀前一定粒度范围颗粒的质量，kg；m 为冲蚀后一定粒度范围颗粒的质量，kg。在颗粒全部破碎时 m=0，也即颗粒破碎程度 f=1。

$$f=\frac{m_0-m}{m_0} \tag{30}$$

2.6　靶面热熔理论

靶面被颗粒撞击时将在几微秒内发生严重塑性变形（应变速率可达 10^3~10^6 s^{-1}[59]），并伴随极强的热效应。当撞击动能足够大时，这种热效应可使靶材去除部分熔化，但热效应对靶面冲蚀损失的影响机制并未被进一步揭示[60-61]。Jennings 等[62]通过冲蚀实验发现，在低冲击速度下，角形颗粒造成的冲蚀速率与球形颗粒存在较大差异；在高冲击速度下，两者的冲蚀速率差异减小。针对角形粒子，高冲击速度产生的冲蚀率并未显著高于低冲击速度的对应值。针对球形粒子，观察到两者存在明显差异，即高速引起的冲蚀速率显著高于低速。这些现象表明，靶面发生冲蚀的程度可能由某个输入能量阈值所控制。当颗粒撞击输出能量超过靶材输入能量阈值后，无论是颗粒速度继续增大，还是颗粒形状发生改变，均不会使冲蚀速率持续变大。通过 SEM 观察典型靶面冲蚀微观形貌（见图 11）发现，撞击区域似乎存在已熔化的碎片及热熔液滴，直观证实了颗粒冲击后，靶面撞击部分发生了热熔，并会流动。Wood[63]发现，靶面宏观力学特性（极限抗拉强度、屈服强度和硬度）并未对冲蚀行为产生显著影响，相反，具有不同热特性的靶面冲蚀行为表现出较大差异。以上研究均表明，在冲蚀过程中，靶面热熔的影响至关重要，靶面输入能量阈值决定靶面热熔是否发生。基于此，相继提出靶面热熔理论及热熔机制影响下的材料冲蚀预测模型，见式（31）[64]。考虑到不同材料的热熔阻力不尽相同，因此该模型对不同靶面材料的适用性仍需进一步探讨。此外，通过 SEM 在撞击区域观察到大量的挤压唇或突出脊，且这种突出脊很容易被后续颗粒撞击，产生变形折断（如图 12 所示），因此可认为材料冲蚀过程由热效应和力学作用两者共同主导，两者对冲蚀的相对贡献目前仍无定论[65]。

$$E_v=\left(\frac{k_T^{5/2}}{F_s}-\frac{G^{1/3}}{\rho_t^{1/3}k_tT_{melt}\Delta H_m}\right)S_v \tag{31}$$

式中：k_T 为单位质量颗粒撞击转移至靶面的动能，J；G 为靶面材料分子质量；k_t 为靶面材料的热导率，W/(m·K)；ΔH_m 为靶面材料的热熔焓，kJ/mol；S_v 为无量纲比例因子。

综上所述，冲蚀理论的出发点和侧重点各异，如

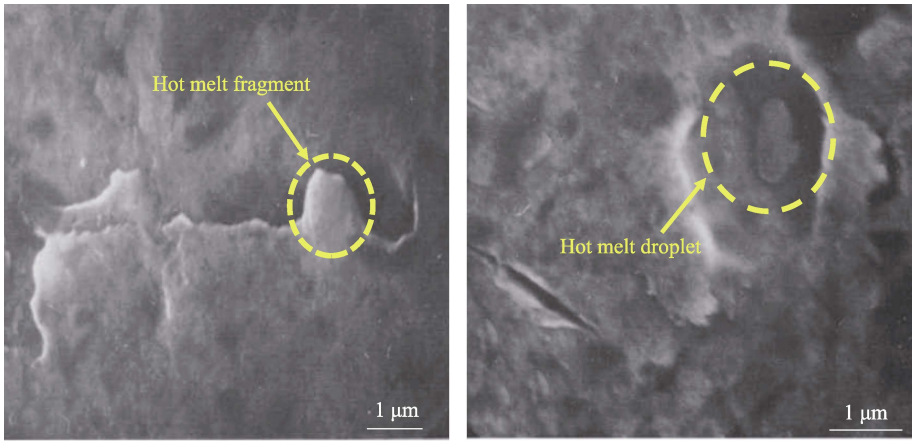

a 靶面形成的热熔碎片　　b 靶面形成的热熔液滴

图 11　靶面冲蚀后的热熔（热激发）微观形貌[62]

Fig.11 Micro morphology of hot melt (thermal excitation) on the target surface after erosion[62]:
a) hot melt fragments formed in the impact part of the target due to high temperature;
b) hot melt droplets formed in the impact part of the target due to high temperature

微切削理论侧重于低攻角下靶面的切削；变形切削理论将高攻角下的靶面变形纳入考虑范畴；挤压–薄片剥落及局部变形理论倾向于解释颗粒撞击靶面形成的软化畸形薄片/变形唇片；二次冲蚀理论重点讨论具有破碎倾向脆性颗粒撞击产生的冲蚀形貌；靶面热熔理论着重分析颗粒撞击热效应对靶面冲蚀的影响机制。这些冲蚀理论的优缺点如表 5 所示。不难发现，这些冲蚀理论均未提及陆地及海上储气库多周期高强度循环注采对管柱冲蚀的影响，因此有必要针对循环注采工况下的管柱冲蚀理论进行发展与完善，这是专家学者亟需开展的研究，也是提高储气库管柱冲蚀预测精度的重点。

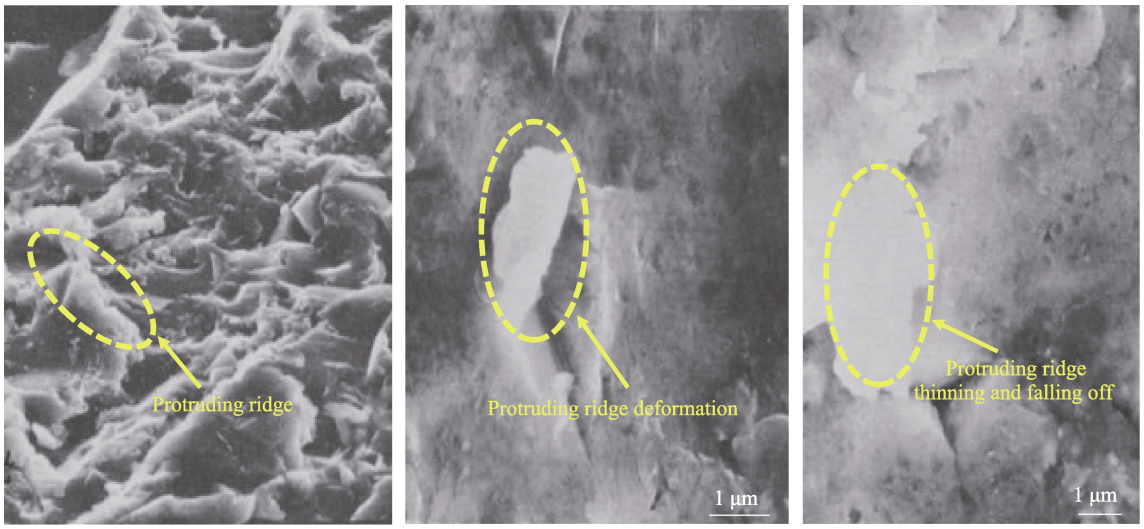

a 颗粒冲击和挤压作用下靶面形成突出脊　b 突出脊发生变形　c 变形突出脊的脱落

图 12　靶面材料冲蚀后的突出脊（机械激发）微观形貌[63-65]

Fig.12 Micro morphology of protruding ridge (mechanically excited) after erosion[63-65]: a) prominent ridge formed under the impact and squeeze of particles; b) protruding ridge deformed by subsequent particle collision; c) deformed protruding ridge falling off due to continuous particle collision

表 5　塑性材料冲蚀理论优缺点汇总

Tab.5 Summary of advantages and disadvantages of plastic material erosion theory

Serial number	Erosion theory model	Advantage	Disadvantage
1	Micro cutting theory	The prediction of low erosion angle is more accurate	The prediction error of high erosion angle is large, and the surface hardening of the target is not considered
2	Deformation and cutting theory	The prediction of high erosion angle is more accurate	There are many empirical coefficients and a priori, and the expansibility is poor
3	Forging extrusion theory	It can effectively explain the flake and falling off process of plastic materials on the target surface under particle impact	The erosion theory does not form an effective erosion prediction model
4	Local deformation theory	It can well evaluate the effect of strain rate and temperature rise on erosion rate	It is only applicable to targets vulnerable to adiabatic shear failure
5	Secondary erosion theory	The erosion prediction of brittle particles under large particle size and high velocity is more accurate.	It is not applicable to material erosion under small particle size and low speed, and the critical particle size and speed are difficult to determine
6	Hot melt on target	The effect of thermal effect produced by particles impacting the target surface on erosion is mainly explained	The applicability of various target materials has not been further discussed

3　管柱冲蚀预测方法

上述冲蚀机理主要针对大类塑性材料提出，关于储气库管柱特定塑性材料的冲蚀预测不可避免地需要借助冲蚀实验系统进行特定工况的冲蚀实验，基于实验结果建立相应的经验性冲蚀预测模型，然后基于 CFD、人工智能等手段实现管柱实际生产工况下的管柱冲蚀程度预测。

3.1　冲蚀实验系统

储气库管柱在强采强注条件下的流动工况复杂多变，使得管柱冲蚀具有极强的环境依赖性且影响因

素众多（见表 6），这些因素可能存在一定的交互作用，导致不同工况下冲蚀预测模型的理论推导难度极大。鉴于此，物理实验系统成为实现冲蚀预测、揭示冲蚀机理不可或缺的研究方法。即通过构建冲蚀实验系统，开展不同工况下的冲蚀实验，将固相颗粒、含颗粒流体及靶面材料属性的待定参数与 E_R 联系起来，实现冲蚀经验或半经验预测模型的建立。然而，目前国内外尚未形成针对冲蚀实验系统的成熟标准及实验规范，不同的实验结果多适用于特定实验流程及实验系统，未系统地研究管柱冲蚀规律，不同工况下实验现象及冲蚀机理的统一解释、冲蚀预测普适模型的建立仍未实现，因此深入研究冲蚀实验系统极具必要性[66]。典型的冲蚀实验系统如图 13 所示[67-71]，根据实验方法的不同，实验系统可分为旋转式、射流式、管流式、单颗粒冲蚀式等，冲蚀实验系统的优劣势及适用性如表 7 所示[20,67,72]。其中，针对冲蚀表征指标 $\overline{E}$，实验系统可采用称量法、超声波法[73-74]、电阻探针法[75]、SEM 法[76]、轮廓法[77-78]、X 射线衍射仪[79]、计算机视觉[80-81]等方法进行测量计算。

表 6　靶面冲蚀的影响参数
Tab.6 Impact parameters of target erosion

Attribute	Influence parameters
Particle	Particle shape, Particle concentration, Particle size, Particle type, Impact velocity, Impact angle etc
Particle with fluid	Temperature, Pressure, Density etc
String material	Density, Hardness, Ductility etc

3.2　冲蚀预测经验模型

上述理论模型有助于了解颗粒撞击过程中的靶面行为及表征冲蚀机制，但不擅长预测特定条件下的靶面冲蚀程度[49]。与上述理论模型不同，冲蚀预测经验模型是在冲蚀实验结果基础上建立的，对不同影响因素下靶面冲蚀率的实验测量结果进行拟合，得到预测模型的因素指数和经验常数。由此可见，经验模型能很好地胜任具体流动条件下靶面冲蚀的预测工作，但目前较少涉及仍未具体定论的靶面冲蚀机制[67]。

常用的冲蚀预测经验模型及其优缺点如表 8 所示[30-31,82-94]。其中，使用频率最高的是 E/CRC 模型和 Oka 模型[95]。E/CRC 模型是美国塔尔萨大学冲蚀/腐蚀研究中心基于大量颗粒撞击靶面的物理实验及数模实验提出的，该模型主要表征颗粒速度、攻角、颗粒形状、靶材硬度对冲蚀的影响，对于以气体为颗粒载体的靶面冲蚀的适用性较强。Oka 等[88]针对铝、铜、碳钢、不锈钢等塑性材料，研究了颗粒速度、攻角、颗粒粒径、颗粒形状、靶面硬度等参数对靶面冲蚀的影响，认为靶面硬度是靶材对颗粒速度和攻角产生依赖性的因变量，该模型适用于任意撞击条件和任何靶材的冲蚀预测。由于以上经验模型基于冲蚀实验，并未考虑高温高压流体的具体影响，因此是否适用于强采强注的储气库管柱仍需进一步探究[96]。与这些复杂的经验性模型不同，简单且高效的预测模型是生产现场所需的。鉴于此，API RP 14E 模型和 Salama 模型成为现场粗略估计管柱冲蚀程度的首选[21,97-98]。当井底有积液时，管柱内易呈现气液固多相流，此时气液

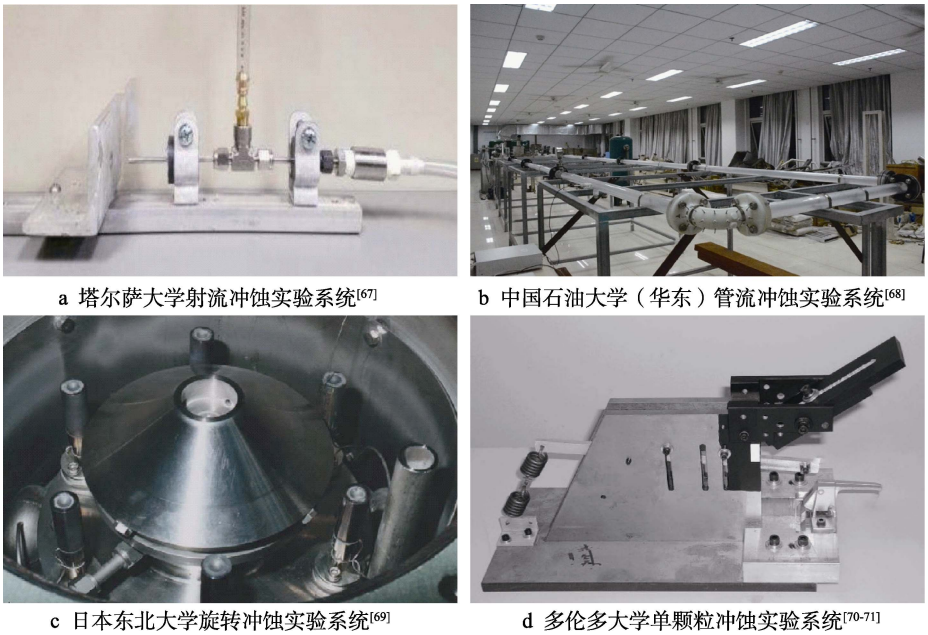

a 塔尔萨大学射流冲蚀实验系统[67]　b 中国石油大学（华东）管流冲蚀实验系统[68]

c 日本东北大学旋转冲蚀实验系统[69]　d 多伦多大学单颗粒冲蚀实验系统[70-71]

图 13　典型的材料冲蚀实验系统

Fig.13 Typical material erosion experimental system: a) jet erosion system in Tulsa University[67]; b) pipe flow erosion system in China University of Petroleum (East China)[68]; c) rotary erosion system in Tohoku University[69]; d) single particle erosion system in University of Toronto[70-71]

表 7 冲蚀实验系统的优劣势及适用性

Tab.7 Advantages and disadvantages and applicability of erosion experimental system

Erosion experiment system	Operating principle	Advantage and disadvantage	Applicability
Rotary type	The sample on the rotating disk rotates at high speed in the slurry containing particles, and erosion occurs with it	Advantage: High stability, Simple operation, Carry out multiple sample erosion at the same time, The test cycle is short. Disadvantage: Eddy current is easily generated in the equipment, which affects the accuracy of erosion experimental data	Mainly for liquid-solid two-phase flow erosion
Jet type	The negative pressure generated by high-speed air flow carries particles and makes them hit the target surface at high speed	Advantage: Simple structure, Convenient parameter adjustment, Produce erosion results in a short time. Disadvantage: It is far from the actual working condition, The degree of target erosion is usually overestimated, The experiment needs to be assisted by high-speed camera, PIV and other devices	Mainly for gas-solid two-phase flow
Pipe flow type	The continuous phase flowing at high speed in the pipe string drives the discrete phase to move and collides with the pipe wall to produce wear	Advantage: It can simulate the real flow conditions of pipe string to the greatest extent, and has good hydrodynamic model support. Disadvantage: The experimental site is usually large, High experimental cost, There is a great demand for gas flow	It is suitable for liquid-solid two-phase flow or gas-liquid-solid multiphase flow erosion
Single particle type	The elastic energy is converted into particle kinetic energy by spring pressure arm device to impact the target surface	Advantage: It can effectively study the influence of impact parameters (impact velocity, impact angle, etc.) on impact behavior and material deformation mechanism, and realize the tracking of particle trajectory. Disadvantage: The experimental particles need self-processing, and the cost of the device is high	Only applicable to single particle impact erosion

分布、砂粒与液滴、液膜间的相互作用将不可忽略，并成为解释砂粒运移特性、追踪砂粒及确定撞击速度的关键。换言之，多相流冲蚀预测的准确性主要取决于多相流模型的准确性[96]。显而易见，气液固多相流与气固两相流冲蚀相比，其建模难度呈指数级上升。目前，国内外针对管线多相流冲蚀的处理方法主要有 2 种方法：基于气固两相流下的冲蚀实验数据开发多相流冲蚀预测模型[99-100]；基于每相“有效直径”将多相流划分为不同组成部分，进行每相冲蚀速率的计算，并相加，即为总冲蚀速率[101]。这 2 种方法的处理结果与实际工况下多相流冲蚀的观察结果仍有一定的误差。

总之，管柱塑性材料冲蚀机理尚无统一表述，由冲蚀样品微观形貌向宏观冲蚀模型转化的速度极为缓慢，建立的验证模型较为不足。换言之，模型参数的取值过度依赖实验数据拟合，而非冲蚀机理，导致模型仅对实验所探究的工况具有适用性，针对其他工况的普适性较差[102]。储气库管柱受到高温、高压、循环交变载荷等其他复杂条件的耦合作用，现场的复杂工况难以通过实验复现，实验结果难以贴合现场。更重要的是，目前冲蚀预测经验模型多针对具体的塑性材料及油气行业集输管线提出，针对储气库管柱强采强注的多相流冲蚀分析及预测目前仍未见报道。

3.3 基于 CFD 的冲蚀预测

上述经验模型可直接用来预测简单几何形状及流动工况下的靶面冲蚀情况，但面对复杂生产工况的储气库管柱则力不从心。得益于计算机计算能力的进步，基于流体动力学（CFD）的冲蚀预测方法应运而生，该工具很容易获取复杂工况下不同参数对靶面冲蚀程度及冲蚀危险位置的影响关系[87]。经过多年的发展，基于 CFD 的冲蚀预测已形成以下 4 个成熟的操作流程，如图 14 所示[96,91,103-104]。

1）建模与网格划分。作为管柱冲蚀分析的第 1 步，几何建模与网格划分能有效解决复杂几何形状及复杂流动条件的表征难题。为了确保冲蚀结果与网格划分无关，在划分网格后必须进行网格敏感性的相关研究[95,105]。

2）管柱流场计算。管柱流场（主要为管内压力、速度、密度、湍动能等参数）的获取主要借助 CFX、FLUENT、STAR-CCM$^+$等 CFD 软件。针对气体动力学基本控制方程及湍流方程的计算，前者遵循气流流动对质量守恒、动量守恒及能量守恒定律，体现为 Navier-Stokers 方程的求解，后者主要涉及湍流模型（标准 k−ε 模型、RNG k−ε 模型、k−ω 模型、RSM 模型、SST 模型等）的合理选取[95,106]。

3）砂粒运动轨迹追踪。砂粒运动的主要计算方法有欧拉−欧拉法和欧拉−拉格朗日法，两者的原理及优缺点见表 9[107-108]，目前后者的使用频率较高。明确砂粒的受力状态是追踪其运动轨迹的基础，通常情况下管柱多相流中固相砂粒会受到拖曳力、压力梯度力、附加质量力、重力与浮力的合力等其他力的作用，分别见式（32）—（35）。确定砂粒的受力情况后，基于牛顿第二定律可得拉格朗日坐标系下单位质量

表 8　常用的冲蚀预测经验模型及其优缺点

Tab.8 Common erosion prediction empirical models and their advantages and disadvantages

Model	Expression	Consider parameters	Advantages and disadvantages
DNV[30]	$\Delta\dot{E}_{\mathrm{m}}=\dot{m}_{\mathrm{p}}\cdot C\cdot v_{\mathrm{p}}^{n}\cdot F(\alpha)$	Particle velocity, Angle of attack	Parameters such as particle shape and particle size are not considered
Mclaury[82-83]	$E_{\mathrm{R}}=C\cdot F_{\mathrm{s}}\cdot v_{\mathrm{p}}^{n}\cdot F(\alpha)$	Particle velocity, Angle of attack, Particle shape	Parameters such as particle size effect and target surface hardness are not considered
Tabakoff[84-85]	$E=K_1\cdot F(\alpha)\cdot v_{\mathrm{p}}^{n}\cdot\cos^2\alpha*(1-R_{\mathrm{T}}^2)+F(v_{\mathrm{in}})$ $R_{\mathrm{T}}=1-0.001\,6v_{\mathrm{p}}\sin\alpha$ $F(\alpha)=\{1+C(K_2\sin(90/\alpha_0)\alpha)\}^2$ $F(v_{\mathrm{in}})=K_3(v_{\mathrm{p}}\sin\alpha)^4$	Particle velocity, Angle of attack, Tangential recovery, Coefficient of particles	The model describes the tangential recovery coefficient of circular particles at small and large angles of attack, which is suitable for the prediction of target erosion at any angle of attack
E/CRC[86-87]	$E_{\mathrm{R}}=k\cdot F_{\mathrm{s}}\cdot v_{\mathrm{p}}^{n}\cdot F(\alpha)\qquad k=C(B_{\mathrm{H}})^{-0.59}$ $B_{\mathrm{H}}=\dfrac{H_{\mathrm{t}}+0.102\,3}{0.010\,8}\qquad F(\alpha)=\sum C_i\alpha^i$	Particle velocity, Angle of attack, Particle shape, Target surface hardness	Without considering the effect of particle size, the prediction accuracy of particle velocity > 50 m/s in large particle size and gas-solid two-phase flow is high
Oka[88]	$E_{\mathrm{v}}(\alpha)=F(\alpha)E_{90^\circ}$ $F(\alpha)=\dfrac{1}{F(\alpha)_{\max}}(\sin\alpha)^{n_1}(1+H_{\mathrm{t}}(1-\sin\alpha))^{n_2}$ $E_{90^\circ}=KH_{\mathrm{t}}^{k1}\left(\dfrac{v_p}{v'}\right)^{k_2}\left(\dfrac{d_p}{d'}\right)^{k_3}$	Particle velocity, Angle of attack, Particle size, Target surface hardness, Particle shape, Particle hardness. ect	Applicable to various particle shapes and various targets; However, the value of empirical parameters depends on the target hardness, and the prediction accuracy of particle velocity > 50 m/s in gas-solid two-phase flow is higher
Nsoesie[89]	$E_{\mathrm{R}}=\dfrac{Cd_{\mathrm{p}}^3\{v_{\mathrm{p}}[A(\sin(\alpha/2))^{1/3}]^B\}^3\rho_{\mathrm{p}}^{3/2}}{H_{\mathrm{t}}^{3/2}}$	Particle velocity, Angle of attack, Particle density, Particle size and target surface hardness	The prediction error of erosion below the critical angle of attack (about 30°) is large
Levin[44]	$E_{\mathrm{R}}\propto E_{\mathrm{parameter}}=$ $\dfrac{mv_{\mathrm{p}}^2}{2}\dfrac{1-\dfrac{3.06\cdot H^{5/4}}{\rho_{\mathrm{p}}\cdot v_{\mathrm{p}}^{1/2}}\cdot\left(\dfrac{1-\mu_{\mathrm{t}}^2}{E_{\mathrm{t}}}+\dfrac{1-\mu_{\mathrm{t}}^2}{E_{\mathrm{p}}}\right)}{T\cdot L}$	Target surface tensile toughness, Plastic area volume, Target surface hardness, Particle density, Particle velocity, Poisson coefficient and elastic modulus of particles and target, Poisson coefficient and elastic modulus of particles and target	The experimental measurement of multi parameters is difficult
API RP 14E[31]	$v_{\mathrm{e}}=\dfrac{C}{\sqrt{\rho_{\mathrm{m}}}}$	Fluid mixing density	The prediction accuracy mainly depends on the value of empirical coefficient C. establishing the corresponding relationship between actual working conditions and C value requires a lot of field data
Salama[90]	$v_{\mathrm{e}}=s\dfrac{D\sqrt{\rho_{\mathrm{m}}}}{\sqrt{W_{\mathrm{p}}}}\qquad E_{\mathrm{R}}=1.86\times10^5\dfrac{W_{\mathrm{p}}}{H_{\mathrm{t}}}\dfrac{v_{\mathrm{p}}^2}{D^2}$	Particle mass flow, Fluid velocity, Bend diameter, Bend target hardness	It is mainly applicable to the erosion prediction of gas-liquid two-phase flow elbow containing sand
FLUENT Software[91]	$E_{\mathrm{R}}=\sum_{p=1}^{N}\dfrac{\dot{m}_pCd_pF(\alpha)v_p^{b(v)}}{A_{\mathrm{face}}}$	Particle size, Angle of attack, Particle velocity, Particle concentration	Particle hardness and material properties of target surface are not considered
Shirazi [92-94]	$h=F_{\mathrm{m}}\cdot F_s\cdot F_{\mathrm{p}}\cdot F_{r/D}\cdot\dfrac{W_{\mathrm{p}}v_{\mathrm{p}}^{1.73}}{(D/D_0)^2}$ $F_{r/D}=\exp\left(-\left(0.1\dfrac{\rho_{\mathrm{f}}^{0.4}\mu_{\mathrm{f}}^{0.65}}{d_{\mathrm{p}}^{0.3}}+0.015\rho_{\mathrm{f}}^{0.25}+0.12\right)(r_{\mathrm{c}}-1.5)\right)$	Impact factor, Particle flow, Particle velocity, Bend diameter, Bend geometry	Without considering the influence of turbulence on particle trajectory, the erosion prediction accuracy of low-density particles in high-density fluid is low

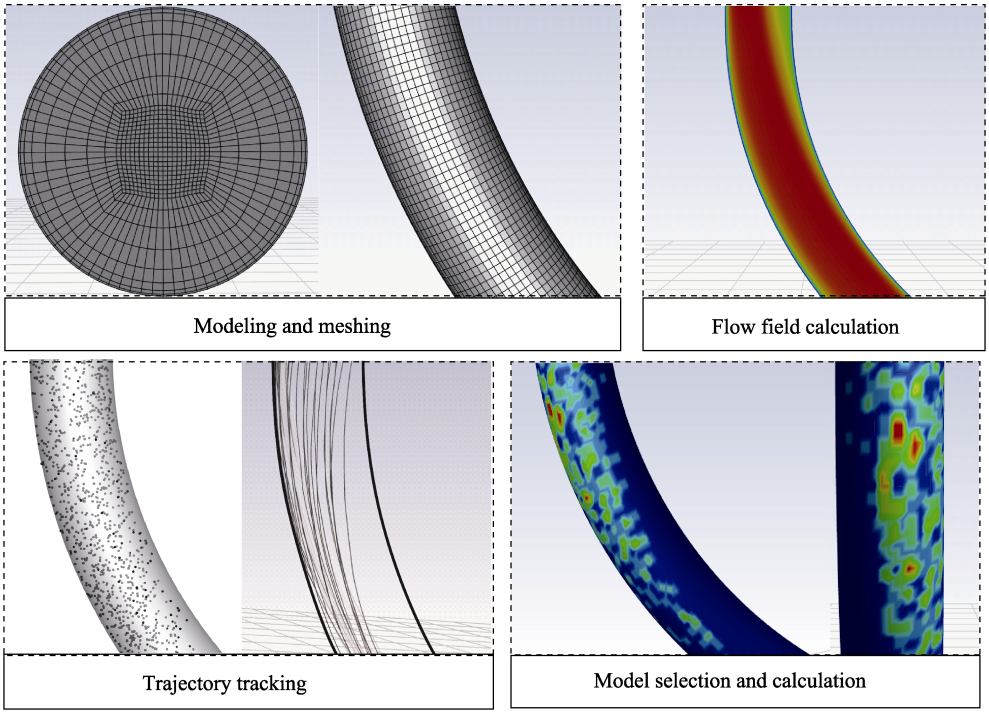

图 14　基于 CFD 预测冲蚀的操作流程

Fig.14 Operation flow of erosion prediction based on CFD

表 9　颗粒运动主流计算方法的原理及优缺点[107-108]

Tab.9 Principle, advantages and disadvantages of mainstream calculation method for particle motion[107-108]

Computing method	Principle	Advantages and disadvantages
Euler-Euler	The gas phase is regarded as a continuous phase and the particles as a continuous pseudo fluid. The gas phase and solid phase are calculated by imitating the single-phase flow in the Euler coordinate system	It is applicable to the working condition with high particle concentration. It is difficult to determine the properties such as particle size and density. Only the average value of particle momentum in a single control unit is given, and the prediction accuracy of particle velocity may be low
Euler-Lagrange	The gas phase is regarded as a continuous phase and the particle as a discrete phase. There is interaction between the gas phase and the solid phase. The Navier Stokes equation of the continuous phase is solved in the Euler coordinate system and the motion control equation of the dissociated phase is solved in the Lagrange coordinate system	This method has high prediction accuracy for particle velocity, but the calculation time is long, DPM model in fluent simulation software adopts this method with high frequenc

砂粒的运动控制方程，见式（36），通过对运动方程进行积分即得到砂粒的运动轨迹[95]。需注意储气库管柱多相流中砂粒与液滴，砂粒与液膜之间的相互作用不可忽略，且管柱液滴夹带率、液滴直径、液膜厚度等参数均会在一定程度上改变砂粒的运动轨迹及靶面的冲蚀程度，这是准确预测储气库管柱冲蚀速率亟需突破的难点之一[18,109-112]。

$$\overrightarrow{F_{\mathrm{D}}}=\frac{18\mu}{\rho_{\mathrm{p}}d_{\mathrm{p}}^{2}}\frac{C_{\mathrm{d}}Re_{\mathrm{s}}}{24}(\overrightarrow{\mu_{\mathrm{f}}}-\overrightarrow{\mu_{\mathrm{p}}}) \tag{32}$$

$$\overrightarrow{F_{\mathrm{p}}}=\frac{\rho_{\mathrm{m}}}{\rho_{\mathrm{p}}}\nabla p \tag{33}$$

$$\overrightarrow{F_{\mathrm{VM}}}=\frac{0.5\rho_{\mathrm{f}}d(\overrightarrow{\mu_{\mathrm{f}}}-\overrightarrow{\mu_{\mathrm{p}}})}{\rho_{\mathrm{p}}dt} \tag{34}$$

$$\overrightarrow{F_{\mathrm{G}}}=\frac{(\rho_{\mathrm{p}}-\rho_{\mathrm{m}})\vec{g}}{\rho_{\mathrm{p}}dt} \tag{35}$$

$$\frac{\mathrm{d}\overrightarrow{\mu_{\mathrm{p}}}}{\mathrm{d}t}=\overrightarrow{F_{\mathrm{D}}}+\overrightarrow{F_{\mathrm{p}}}+\overrightarrow{F_{\mathrm{VM}}}+\overrightarrow{F_{\mathrm{G}}} \tag{36}$$

式中：$\overrightarrow{F_{\mathrm{D}}}$ 为单位颗粒受到的曳力，N；$\overrightarrow{F_{\mathrm{p}}}$ 为单位颗粒受到的压力梯度力，N；$\overrightarrow{F_{\mathrm{VM}}}$ 为单位质量颗粒受到的附加质量力，N；$\overrightarrow{F_{\mathrm{G}}}$ 为单位颗粒受到的重力和浮力的合力，N；ρ_{f} 为连续相密度，kg/m^3；Re_{s} 为固体颗粒雷诺数；C_{d} 为曳力系数，取值随雷诺数的变化而改变，球形砂粒由亚历山大模型计算，见式（37），a_1、a_2、a_3 为常数），非球形砂粒由文斯皮尔模型计算，见式（38），b_1、b_2、b_3、b_4 为常数；$\overrightarrow{\mu_{\mathrm{p}}}$ 为固体颗粒

的速度矢量，m/s；$\overrightarrow{\mu_f}$ 为瞬时速度矢量，m/s；μ 为黏度，Pa·s。

$$C_d = a_1 + \frac{a_2}{Re_s} + \frac{a_3}{Re_s^2} \tag{37}$$

$$C_d = \frac{24}{Re_s}(1 + b_1 Re_s^{b_2}) + \frac{b_3 Re_s}{b_4 + Re_s} \tag{38}$$

4）冲蚀模型的选取及冲蚀的计算。虽然基于 CFD 的冲蚀计算很容易获得油气集输管柱的冲蚀易发区域及最危险位置，在一定程度上为现场管柱冲蚀预测指明了方向。遗憾的是，目前还无学者在考虑储气库注采管柱埋深大、温压场复杂多变、注采交变载荷、储层出砂等特点的基础上，基于 CFD 手段开展储气库注采管柱冲蚀仿真模拟。原因在于管柱的冲蚀研究采用先选模型后基于实验数据进行模型验证的思路，而储气库注采管柱的现场生产工况难以通过实验模拟得到，抛开实验条件不说，管柱注采期间不可避免地会产生大量不确定的冲蚀数据，且这些数据的真实准确性难以考究，采用确定的冲蚀模型去预测这种不确定的冲蚀结果显然易获得较低的预测精度，这成为基于 CFD 冲蚀预测方法的另一应用缺陷[113]。

3.4　基于人工智能的冲蚀预测

鉴于上述 CFD 冲蚀预测方法的局限性，一些学者引入机器学习算法（人工智能的核心），尝试借助概率模型来处理管柱中不确定的冲蚀数据，以期进一步提高管柱冲蚀率的预测精度[113]。机器学习算法的目标是学习如何使用特征向量（因变量），获取冲蚀预测结果的最优模型。常见的机器学习算法有线性回归（LM）、决策树、支持向量机（SVM）、人工神经网络（ANN）、贝叶斯网络（BN）、随机森林（RF）、遗传算法（GA）等。其中，LM 常用于连续数值的预测，且预测结果具有可解释性，但针对接近 0 且严格为正的数值情况，其预测精度较差；SVM 主要使用径向基函数估计非线性决策面，这会导致噪声数据的过度拟合；在学习训练期间的 ANN 属于黑匣子，其调整难度较大，针对小数据集时 ANN 的预测精度有限，针对大数据集虽然具较高的预测精度，但计算时间较长，对计算资源的要求较高[114-115]；GA 能直接处理冲蚀实验原始数据（靶材质量损失分布及颗粒轨迹数据），常用于冲蚀预测模型的校准[116]。Liu 等[113]对比分析了应用决策树、ANN 和 BN 的管道冲蚀预测结果，发现针对粗略或不确定的冲蚀实验数据，分类树能够快速优化，ANN 擅长对诸多输入参数进行敏感性评估，贝叶斯网络则组合了分类树和 ANN 的优点，通过概率分布能够轻松处理不确定冲蚀数据，并确定其冲蚀率和冲蚀临界速度。RF 作为基于决策树的一种算法，通过拟合多个无关联的决策树来提高平均预测精度，并有效避免过拟合问题。换言之，该算法可以最大程度地利用不同流动工况下的海量实验数据，提高数据价值，现场工况实用性较强[117]。鉴于此，基于 RF 及 201 组各种流动条件下的冲蚀实验数据，Zahedi 等[96]对 90°弯管的冲蚀程度进行了预测，发现 RF 能大大降低冲蚀率的累积误差，并获得了颗粒速度、表面剪切应力、DPM 浓度、湍流动能等 8 个参数对冲蚀率的影响权重。

总之，基于人工智能的冲蚀预测目前正处于探索初级阶段，这种探索性受到机器学习算法选择及其应用设置的诸多限制，因此在进行人工智能推广前应对具体的机器学习算法进行必要且大量的实验验证[113]。此外，无论是基于 CFD 还是人工智能手段，储气库管柱所受强交替作用对冲蚀的具体影响均未被考虑，这是实现储气库冲蚀准确预测的重点、难点。

受限于储气库高温、高压、循环交变载荷等耦合下的管柱复杂注采行为及不成熟的管柱冲蚀理论，难以使用单个模型来准确描述现场储气库管柱是否发生冲蚀及冲蚀的严重程度。鉴于此，我国地下储气库管柱安全分析可采用多个冲蚀表征指标及多个冲蚀预测模型进行计算，然后借助人工智能技术，充分利用现场管柱监测数据，以获得管柱冲蚀发生概率及冲蚀损失程度的范围，尽可能地指导现场安全生产。

4　结语

明晰塑性材料冲蚀机理，基于冲蚀准则及表征指标建立管柱冲蚀预测模型，这对减少储气库建设成本，最大限度发挥储气库管柱服役年限，实现储气库供需调峰、战略储备功能等具有重要的理论指导和现实意义。储气库管柱所受强交替作用对冲蚀的影响是储气库管柱冲蚀理论及预测研究的重中之重。目前，针对储气库强采强注工况下的管柱冲蚀的报道极少，因此管柱冲蚀分析与预测多借鉴塑性材料经典冲蚀理论及气主导体系中管道冲蚀的相关研究成果。

1）经典冲蚀理论解释了颗粒撞击过程中的靶面行为，以及表征了冲蚀机制，但并不擅长预测特定工况下的靶面冲蚀程度。基于实验数据的冲蚀经验预测模型虽能很好地预测具体流动条件下的靶面冲蚀，但却较少涉及冲蚀机理。

2）冲蚀预测经验模型的参数取值过度依赖实验数据拟合而非冲蚀机理，导致经验模型仅对实验所探究的工况具有适用性，针对其他工况的普适性较差。再者，冲蚀预测经验模型多针对油气行业集输管线提出，针对储气库管柱强采强注工况下的多相流冲蚀分析及预测目前仍未见相关报道。

3）基于 CFD 的冲蚀预测方法易计算出管柱的冲蚀易发区域及最危险位置，目前并无指导选取合适冲蚀模型的相关标准或报道，导致冲蚀模型的选取具备一定先验性，这在一定程度限制了该预测方法的拓展。此外，该预测方法并不能处理管柱注采期间产生

的大量不确定性冲蚀数据，管柱冲蚀的预测精度有待商榷。

4）基于人工智能的冲蚀预测，借助概率模型能很好地预测管柱不确定的冲蚀结果，但预测精度仍受到机器学习算法选择及应用设置的诸多限制，且其应用可行性仍需大量实验数据进一步验证。人工智能的引入，无疑为现有冲蚀理论在储气库现场的应用搭建了桥梁，从而更好地利用储气库管柱现场监测数据对多个冲蚀表征指标及冲蚀预测模型进行验证，推动我国储气库建设向智能化方向的发展

参考文献

[1] 中国石油报. 储气库在疫情期间发挥重要作用[EB/OL]. [2020-04-22]. https://cj.sina.com.cn/articles/view/2754683003/va431207b01900s26d?from=finance.
China Petroleum News. Gas Storage Plays an Important Role during the Epidemic[EB/OL]. [2020-04-22]. https://cj.sina.com.cn/articles/view/2754683003/va431207b01900s26d?from=finance.

[2] 刘建勋, 刘岩. 中国地下储气库建设的发展现状及展望[J]. 应用化工, 2022, 51(4): 1136-1140.
LIU Jian-xun, LIU Yan. Development Status and Prospects of China's Underground Gas Storage Construction[J]. Applied Chemical Industry, 2022, 51(4): 1136-1140.

[3] 丁国生, 丁一宸, 李洋, 等. 碳中和战略下的中国地下储气库发展前景[J]. 油气储运, 2022, 41(1): 1-9.
DING Guo-sheng, DING Yi-chen, LI Yang, et al. Prospects of Underground Gas Storage in China under the Strategy of Carbon Neutrality[J]. Oil & Gas Storage and Transportation, 2022, 41(1): 1-9.

[4] 董长银, 陈琛, 周博, 等. 油气藏型储气库出砂机理及防砂技术现状与发展趋势展望[J]. 石油钻采工艺, 2022, 44(1): 43-55.
DONG Chang-yin, CHEN Chen, ZHOU Bo, et al. Sand Production Mechanism and Sand Control Technology Status and Prospect of Oil-Gas Reservoir Type Gas Storage[J]. Oil Drilling & Production Technology, 2022, 44(1): 43-55.

[5] 谭羽非, 班凡生, 李玉星. 天然气地下储气库数值模拟技术[M]. 北京: 石油工业出版社, 2020: 65-69.
TAN Yu-fei, BAN Fan-sheng, LI Yu-xing. Numerical Simulation Technology of Natural Gas Underground Storage[M]. Beijing: Petroleum Industry Press, 2020: 65-69.

[6] 卢斌. 喷射式冲蚀实验装置研制及油井管柱抗冲蚀性能研究[D]. 西安: 西安石油大学, 2012: 20-21.
LU Bin. Design and Manufacture of Jet Test Machine for Erosion and Research on Erosion-Resistance Behavior of Oil Well String[D]. Xi'an: Xi'an Shiyou University, 2012: 20-21.

[7] 丰先艳. 双 6 储气库出砂规律分析[C]// 2018 年全国天然气学术年会论文集(02 气藏开发), 2018: 183-188.
FENG Xian-yan. Analysis on Sand Production Law of Shuang-6 Gas Storage[C]// Proceedings of 2018 National Natural Gas Academic Annual Conference (02 Gas Reservoir Development), 2018: 183-188.

[8] 贺梦琦, 王江宽, 陈显学, 等. 储气库井注采出砂模拟系统及方法: 中国, 112377169A[P]. 2021-02-19.
HE Meng-qi, WANG Jiang-kuan, CHEN Xian-xue, et al. Injection and Sand-Production Simulating System and Method for Gas Storage Well: China, 112377169A[P]. 2021-02-19.

[9] 隋义勇, 林堂茂, 刘翔, 等. 交变载荷对储气库注采井出砂规律的影响[J]. 油气储运, 2019, 38(3): 303-307.
SUI Yi-yong, LIN Tang-mao, LIU Xiang, et al. The Influence of Alternating Load on Sand Production Law of Injection/Production Wells of Underground Gas Storages [J]. Oil & Gas Storage and Transportation, 2019, 38(3): 303-307.

[10] 天工. 我国首个海上储气库群项目开工[J]. 天然气工业, 2021, 41(5): 143.
TIAN Gong. China's First Offshore Gas Storage Group Project Started[J]. Natural Gas Industry, 2021, 41(5): 143.

[11] 汪亚萍, 刘青, 邢利民. 渤海钻探 国内首口海上储气库井顺利入窗[EB/OL]. [2021-08-16]. https://kns.cnki.net/kcms/detail/detail.aspx?FileName=SHYO202108160012&DbName=CCND2021.
WANG Ya-ping, LIU Qing, XING Li-min. Bohai Drilling Successfully Entered the Window of the First Offshore Gas Storage Well in China[EB/OL]. [2021-08-16]. https://kns.cnki.net/kcms/detail/detail.aspx?FileName= SHYO202108160012& DbName=CCND2021.

[12] 中华人民共和国国家发展和改革委员会. 我国首个海上储气库群项目开工[EB/OL]. [2021-05-31]. https://www.ndrc.gov.cn/fggz/jjyxtj/mdyqy/202105/t20210531_1282077_ext.html.
National Development and Reform Commission. China's First Offshore Gas Storage Group Project Started [EB/OL]. [2021-05-31]. https://www.ndrc.gov.cn/fggz/jjyxtj/mdyqy/202105/t20210531_1282077_ext.html.

[13] 曾妍. 我国首个海上储气库群项目开工[J]. 天然气与石油, 2021, 39(4): 136.
ZENG Yan. China's First Offshore Gas Storage Group Project Started[J]. Petrochemical Industry Application, 2021, 39(4): 136.

[14] 何颋婷. 老的裂缝性气藏成为储气库[J]. 天然气勘探与开发, 2019, 42(2): 21.
HE Ting-ting. The Old Fractured Gas Reservoir Becomes a Gas Storage[J]. Natural Gas Exploration and Development, 2019, 42(2): 21.

[15] 李国韬, 刘飞, 宋桂华, 等. 大张坨地下储气库注采工艺管柱配套技术[J]. 天然气工业, 2004, 24(9): 156-158.
LI Guo-tao, LIU Fei, SONG Gui-hua, et al. Matching Techniques of Process Pipe String for Injection and Recovery Wells in Dazhangtuo Underground Gas Storage [J]. Natural Gas Industry, 2004, 24(9): 156-158.

[16] 何祖清, 何同, 伊伟锴, 等. 中国石化枯竭气藏型储气

库注采技术及发展建议[J]. 地质与勘探, 2020, 56(3): 605-613.
HE Zu-qing, HE Tong, YIN Wei-kai, et al. Development Suggestions and Production Technologies and Development of Sinopec's Gas Storage of Depleted Gas Reservoir Type[J]. Geology and Exploration, 2020, 56(3): 605-613.

[17] NAJAFIFARD F. Predicting near Wall Particle Behavior with Application to Erosion Simulation[D]. Tulsa: University of Tulsa, 2014: 114-129.

[18] POSTLETHWAITE J, NEŠIĆ S. Erosion-Corrosion in Single and Multiphase Flow[M]// Uhlig's Corrosion Handbook. Hoboken, NJ, USA: John Wiley & Sons, Inc, 2011: 215-227.

[19] ARABNEJAD KHANOUKI H. Development of Erosion Equations for Solid Particle and Liquid Droplet Impact [D]. Tulsa: University of Tulsa, 2015: 33-39.

[20] RAJKUMAR Y R. Effect of Impact-particle Size, Shape and Velocity on Single Particle Derormation Measurements and Predictions[D]. Oklahoma: University of Tulsa, 2018: 5-10.

[21] 王云, 张建军. 地下储气库注采井临界冲蚀流量优化计算方法[J]. 天然气工业, 2019, 39(11): 74-80.
WANG Yun, ZHANG Jian-jun. An Optimized Calculation Method of Critical Erosion Flow Rates of UGS Injection/ Production Wells[J]. Natural Gas Industry, 2019, 39(11): 74-80.

[22] MADANI SANI F, HUIZINGA S, ESAKLUL K A, et al. Review of the API RP 14E Erosional Velocity Equation: Origin, Applications, Misuses, Limitations and Alternatives[J]. Wear, 2019, 426/427: 620-636.

[23] 张琪, 万仁溥. 采油工程方案设计[M]. 北京: 石油工业出版社, 2002: 292-294.
ZHANG Qi, WAN Ren-pu. Production Engineering Project Design[M]. Beijing: Petroleum Industry Press, 2002: 292-294.

[24] SALAMA M M. An Alternative to API 14E Erosional Velocity Limits for Sand-Laden Fluids[J]. Journal of Energy Resources Technology, 2000, 122(2): 71-77.

[25] RICKERBY D G, MACMILLAN N H. The Erosion of Aluminum by Solid Particle Impingement at Oblique Incidence[J]. Wear, 1982, 79(2): 171-190.

[26] MEDNIKOV A F, RYZHENKOV V A, SELEZNEV L I, et al. Studying the Variation of Parameters Characterizing the Material Surface during the Droplet Erosion Incubation Period[J]. Thermal Engineering, 2012, 59(5): 414-420.

[27] RICKERBY D G, MACMILLAN N H. The Erosion of Aluminum by Solid Particle Impingement at Normal Incidence[J]. Wear, 1980, 60(2): 369-382.

[28] HUTCHINGS I M. A Model for the Erosion of Metals by Spherical Particles at Normal Incidence[J]. Wear, 1981, 70(3): 269-281.

[29] FELLER W. An Introduction to Probability Theory and Its Applications: Volume 2 Second Edition[M]. New York: Wiley, 1991: 87-95.

[30] DNV RP 0501-2007, Recommended Practice, RP O501: Erosive Wear in Piping Systems[S].

[31] API RP 14E, Recommended Practice for Design and Installation of Offshore Production Platform Piping Systems[S].

[32] HAUGEN K, KVERNVOLD O, RONOLD A, et al. Sand Erosion of Wear-Resistant Materials: Erosion in Choke Valves[J]. Wear, 1995, 186/187: 179-188.

[33] FINNIE I. The Mechanism of Erosion of Ductile Metals [C]// 3rd US National Congress of Applied Mechanics, 1958: 527–532.

[34] FINNIE I. Some Reflections on the Past and Future of Erosion[J]. Wear, 1995, 186/187: 1-10.

[35] FINNIE I. Erosion of Surfaces by Solid Particles[J]. Wear, 1960, 3(2): 87-103.

[36] PARSI M, NAJMI K, NAJAFIFARD F, et al. A Comprehensive Review of Solid Particle Erosion Modeling for Oil and Gas Wells and Pipelines Applications[J]. Journal of Natural Gas Science and Engineering, 2014, 21: 850-873.

[37] BUDINSKI K G. Incipient Galling of Metals[J]. Wear, 1981, 74(1): 93-105.

[38] ALAM T, FARHAT Z N. Slurry Erosion Surface Damage under Normal Impact for Pipeline Steels[J]. Engineering Failure Analysis, 2018, 90: 116-128.

[39] HASHISH M. Modified Model for Erosion[C]// Proceedings of the 7th International Conference on Erosion by Liquid and Solid Impact. Cambridge: Robinson College, 1987: 461-480.

[40] HUANG Cun-kui, CHIOVELLI S, MINEV P, et al. A Comprehensive Phenomenological Model for Erosion of Materials in Jet Flow[J]. Powder Technology, 2008, 187(3): 273-279.

[41] BITTER J G A. A Study of Erosion Phenomena Part I[J]. Wear, 1963, 6(1): 5-21.

[42] BITTER J G A. A Study of Erosion Phenomena[J]. Wear, 1963, 6(3): 169-190.

[43] LANKOV A. Erosive Destruction of Materials under Rebounding a Flow of Hard Spherical Particles[J]. Trenie Iznos, 1992, 13(1): 206-221.

[44] LEVIN B F, VECCHIO K S, DUPONT J N, et al. Modeling Solid-Particle Erosion of Ductile Alloys[J]. Metallurgical and Materials Transactions A, 1999, 30(7): 1763-1774.

[45] NEILSON J H, GILCHRIST A. Erosion by a Stream of Solid Particles[J]. Wear, 1968, 11(2): 111-122.

[46] SHELDON G L, KANHERE A. An Investigation of Impingement Erosion Using Single Particles[J]. Wear, 1972, 21(1): 195-209.

[47] SÖDERBERG S, HOGMARK S, SWAHN H. Mechanisms of Material Removal during Erosion of a Stainless Steel[J]. A S L E Transactions, 1983, 26(2): 161-172.

[48] ELTOBGY M S, NG E, ELBESTAWI M A. Finite Element Modeling of Erosive Wear[J]. International Journal of Machine Tools and Manufacture, 2005, 45(11): 1337-1346.

[49] ARABNEJAD H, MANSOURI A, SHIRAZI S A, et al. Development of Mechanistic Erosion Equation for Solid Particles[J]. Wear, 2015, 332/333: 1044-1050.
[50] LEVY A V. The Platelet Mechanism of Erosion of Ductile Metals[J]. Wear, 1986, 108(1): 1-21.
[51] LEVY A V. The Erosion of Structural Alloys, Cermets and *in Situ* Oxide Scales on Steels[J]. Wear, 1988, 127(1): 31-52.
[52] LEVY A V. The Solid Particle Erosion Behavior of Steel as a Function of Microstructure[J]. Wear, 1981, 68(3): 269-287.
[53] SUNDARARAJAN G, SHEWMON P G. A New Model for the Erosion of Metals at Normal Incidence[J]. Wear, 1983, 84(2): 237-258.
[54] REDDY A V, SUNDARARAJAN G. Erosion Behaviour of Ductile Materials with a Spherical Non-Friable Erodent [J]. Wear, 1986, 111(3): 313-323.
[55] CHRISTMAN T, SHEWMON P G. Adiabatic Shear Localization and Erosion of Strong Aluminum Alloys[J]. Wear, 1979, 54(1): 145-155.
[56] 邵荷生, 曲敬信, 许小棣. 摩擦与磨损[M]. 北京: 煤炭工业出版社, 1992: 108-120.
SHAO He-sheng, QU Jing-xin, XU Xiao-di. Friction and Wear[M]. Beijing: China Coal Industry Publishing House, 1992: 108-120.
[57] CHEN Da-nian, SARUMI M, AL-HASSANI S T S, et al. A Model for Erosion at Normal Impact[J]. Wear, 1997, 205(1/2): 32-39.
[58] TILLY G P. A Two Stage Mechanism of Ductile Erosion [J]. Wear, 1973, 23(1): 87-96.
[59] HUTCHINGS I M. Strain Rate Effects in Microparticle Impact[J]. Journal of Physics D: Applied Physics, 1977, 10(14): L179-L184.
[60] FINNIE I. Some Observations on the Erosion of Ductile Metals[J]. Wear, 1972, 19(1): 81-90.
[61] NEILSON J H, GILCHRIST A. An Experimental Investigation into Aspects of Erosion in Rocket Motor Tail Nozzles[J]. Wear, 1968, 11(2): 123-143.
[62] JENNINGS W H, HEAD W J, MANNING C R. A Mechanistic Model for the Prediction of Ductile Erosion [J]. Wear, 1976, 40(1): 93-112.
[63] WOOD C D. Erosion of Metals by the High Speed Impact of Dust Particles[C]// Annual Technical Meeting Proceedings, San diego: Institute of Environment Science, 1966: 55-63.
[64] SMELTZER C E, GULDEN M E, MCELMURY S S, et al. Mechanisms of Sand and Dust Erosion in Gas Turbing Engines[M]. Fort Eustis: Army Air Mobility Research and Development Laboratory, 1970: 57-70.
[65] HUTCHINGS I M. Mechanisms of the Erosion of Metals by Solid Particles[M]. Erosion: Prevention and Useful Applications, 2009: 59-76.
[66] ASTM G76-13, Standard Test Method for Conducting Erosion Tests by Solid Particle Impingement Using Gas Jets[S].
[67] HAIDER G. Mechanistic Modelling for Rebound of Solid Particles with Applications to Erosion Predictions[D]. Oklahoma: University of Tulsa, 2017: 19-30.
[68] 彭文山. 含固体颗粒多相流弯管冲蚀机理研究[D]. 东营: 中国石油大学(华东), 2017: 15-17.
PENG Wen-shan. Study on the Solid Particle Erosion Mechanism of Pipe Bend for Multiphase Flow[D]. Dongying: China University of Petroleum (Huadong), 2017: 15-17.
[69] HAYASHI N, KAGIMOTO Y, NOTOMI A, et al. Development of New Testing Method by Centrifugal Erosion Tester at Elevated Temperature[J]. Wear, 2005, 258 (1/2/3/4): 443-457.
[70] DHAR S, KRAJAC T, CIAMPINI D, et al. Erosion Mechanisms Due to Impact of Single Angular Particles [J]. Wear, 2005, 258(1/2/3/4): 567-579.
[71] XIE Zhen-qiang, CAO Xue-wen, FU Chen-yang, et al. Experimental Study on the Repeated Impact of Sharp Particles on Metal Surface[J]. Wear, 2021, 474/475: 203716.
[72] BURNETT A J, BRADLEY M S A, O'FLYNN D J, et al. Anomalies in the Results Obtained from Rotating Disc Accelerator Erosion Testers: A Discussion of Possible Causes[J]. Wear, 1999, 233/234/235: 275-283.
[73] HONARVAR F, SALEHI F, SAFAVI V, et al. Ultrasonic Monitoring of Erosion/Corrosion Thinning Rates in Industrial Piping Systems[J]. Ultrasonics, 2013, 53(7): 1251-1258.
[74] PARSI M, VIEIRA R E, KESANA N, et al. Ultrasonic Measurements of Sand Particle Erosion in Gas Dominant Multiphase Churn Flow in Vertical Pipes[J]. Wear, 2015, 328/329: 401-413.
[75] VIEIRA R E, PARSI M, ZAHEDI P, et al. Electrical Resistance Probe Measurements of Solid Particle Erosion in Multiphase Annular Flow[J]. Wear, 2017, 382/383: 15-28.
[76] 耿明睿, 陈皎, 杨竹芳, 等. TC4 钛合金表面冲蚀损伤机理的砂尘粒径依赖效应[J]. 中国表面工程, 2018, 31(3): 17-26.
GENG Ming-rui, CHEN Jiao, YANG Zhu-fang, et al. Dependent Effects of Particle Size on Erosion Wear Mechanism of TC4 Titanium Alloy[J]. China Surface Engineering, 2018, 31(3): 17-26.
[77] KARIMI S, MANSOURI A, SHIRAZI S A, et al. Experimental Investigation on the Influence of Particle Size in a Submerged Slurry Jet on Erosion Rates and Patterns[C]// Proceedings of ASME 2017 Fluids Engineering Division Summer Meeting, 2017: 7-9.
[78] OKONKWO P C, SLIEM M H, HASSAN SK M, et al. Erosion Behavior of API X120 Steel: Effect of Particle Speed and Impact Angle[J]. Coatings, 2018, 8(10): 343.
[79] 李玉琴, 文建中, 孙志平. TC4 钛合金表面 TiAlN/Ti 涂层的抗冲蚀性能研究[J]. 表面技术, 2021, 50(7): 276-282.
LI Yu-qin, WEN Jian-zhong, SUN Zhi-ping. Study on Erosion Resistance of the TiAlN/Ti Coating for TC4

Titanium Alloy[J]. Surface Technology, 2021, 50(7): 276-282.

[80] KIM H S, LEE B R. Real-Time Pipe Fault Detection System Using Computer Vision[J]. International Journal of Precision Engineering and Manufacturing, 2006, 7(1): 30-34.

[81] BAILEY D, JONES M, TANG Li-qiong. Real Time Vision for Measuring Pipe Erosion[C]// The 5th International Conference on Automation, Robotics and Applications. Wellington, New Zealand. IEEE, 2012: 486-491.

[82] CHEN Xiang-hui, MCLAURY B S, SHIRAZI S A. Application and Experimental Validation of a Computational Fluid Dynamics (CFD)-Based Erosion Prediction Model in Elbows and Plugged Tees[J]. Computers & Fluids, 2004, 33(10): 1251-1272.

[83] MCLAURY B S. Predicting Solid Particle Erosion Resulting from Turbulent Fluctuations in Oilfield Geometries [D]. Tulsa: University of Tulsa, 1996: 77-82.

[84] TABAKOFF W, KOTWAL R, HAMED A. Erosion Study of Different Materials Affected by Coal Ash Particles[J]. Wear, 1979, 52(1): 161-173.

[85] GRANT G, BALL R, TABAKOFF W. An Experimental Study of the Erosion Rebound Characteristics of High Speed Particles Impacting a Stationary Specimen[M]. State of Ohio: University of Cincinnati Technical Report, 1973: 104-107.

[86] AHLERT K R. Effects of Particle Impingement Angle and Surface Wetting on Solid Particle Erosion of AISI 1018 Steel[D]. Oklahoma: University of Tulsa, 1994: 75-80.

[87] ZHANG Y, REUTERFORS E P, MCLAURY B S, et al. Comparison of Computed and Measured Particle Velocities and Erosion in Water and Air Flows[J]. Wear, 2007, 263(1/2/3/4/5/6): 330-338.

[88] OKA Y I, OKAMURA K, YOSHIDA T. Practical Estimation of Erosion Damage Caused by Solid Particle Impact Part 1: Effects of impact parameters on a predictive equation[J]. Wear, 2005, 259(1/2/3/4/5/6): 95-101.

[89] NSOESIE S, LIU R, CHEN K Y, et al. Analytical Modeling of Solid-Particle Erosion of Stellite Alloys in Combination with Experimental Investigation[J]. Wear, 2014, 309(1/2): 226-232.

[90] SALAMA M M, VENKATESH E S. Evaluation of API RP 14E Erosional Velocity Limitations for Offshore Gas Wells[C]// Offshore Technology Conference. Houston, Texas. Offshore Technology Conference, 1983: 371-375.

[91] MOUKETOU F N, KOLESNIKOV A. Modelling and Simulation of Multiphase Flow Applicable to Processes in Oil and Gas Industry[J]. Chemical Product and Process Modeling, 2018, 14(1): 20170066.

[92] SHIRAZI S A, SHADLEY J R, MCLAURY B S, et al. A Procedure to Predict Solid Particle Erosion in Elbows and Tees[J]. Journal of Pressure Vessel Technology, 1995, 117(1): 45-52.

[93] MANSOURI A. A Combined CFD-Experimental Method for Developing an Erosion Equation for both Gas-Sand and Liquid-Sand Flows[D]. Tulsa: University of Tulsa, 2016: 75-78.

[94] BOURGOYNE A T Jr. Experimental Study of Erosion in Diverter Systems Due to Sand Production[C]// SPE/IADC Drilling Conference. New Orleans, Louisiana. Society of Petroleum Engineers, 1989: 807-816.

[95] FAROKHIPOUR A, MANSOORI Z, SAFFAR-AVVAL M, et al. 3D Computational Modeling of Sand Erosion in Gas-Liquid-Particle Multiphase Annular Flows in Bends[J]. Wear, 2020, 450/451: 203241.

[96] ZAHEDI P, PARVANDEH S, ASGHARPOUR A, et al. Random Forest Regression Prediction of Solid Particle Erosion in Elbows[J]. Powder Technology, 2018, 338: 983-992.

[97] 王嘉淮, 罗天雨, 吕毓刚, 等. 呼图壁地下储气库气井冲蚀产量模型及其应用[J]. 天然气工业, 2012, 32(2): 57-59.
WANG Jia-huai, LUO Tian-yu, LYU Yu-gang, et al. Research and Application of the Model of Gas Well Erosion Output of the Hutubi Underground Gas Storage [J]. Natural Gas Industry, 2012, 32(2): 57-59.

[98] 张智, 冯潇霄, 向世林. 高温高产气井冲蚀对油管柱结构完整性的影响[J]. 中国科技论文, 2022, 17(1): 31-38.
ZHANG Zhi, FENG Xiao-xiao, XIANG Shi-lin. Influence of High Temperature and High Yield Gas Well Erosion on Structural Integrity of Oil String[J]. China Sciencepaper, 2022, 17(1): 31-38.

[99] MCLAURY B S, SHIRAZI S A. An Alternate Method to API RP 14E for Predicting Solids Erosion in Multiphase Flow[J]. Journal of Energy Resources Technology, 2000, 122(3): 115-122.

[100] MCLAURY B, RYBICKI E, SHIRAZI S, et al. How Operating and Environmental Conditions Affect Erosion [C]// NACE International Annual Conference. Houston: NACE International, 1999: 34.

[101] JORDAN K G. Erosion in Multiphase Production of Oil & Gas[C]//NACE International Annual Conference. Houston: NACE International, 1998: 58.

[102] MENG H C, LUDEMA K C. Wear Models and Predictive Equations: Their Form and Content[J]. Wear, 1995, 181/182/183: 443-457.

[103] 张晴波, 郭涛, 洪国军, 等. 喷砂冲蚀实验中颗粒轨迹的数值预测[J]. 爆炸与冲击, 2021, 41(2): 158-165.
ZHANG Qing-bo, GUO Tao, HONG Guo-jun, et al. Numerical Prediction of Particle Trajectories in an Erosion Experiment[J]. Explosion and Shock Waves, 2021, 41(2): 158-165.

[104] ABDULLA A. Estimation Erosion in Oil and Gas Pipe line due to Sand Presence[D]. Karlskrona: Blekinge Institute of Technology, 2011: 41-49.

[105] ZHANG Jun, MCLAURY B S, SHIRAZI S A. Modeling Sand Fines Erosion in Elbows Mounted in Series[J]. Wear, 2018, 402/403: 196-206.

[106] ZHANG R, LIU H X. Numerical Simulation of Solid

Particle Erosion in a 90 Degree Bend for Gas Flow[C]// Proceedings of ASME 2014 33rd International Conference on Ocean, Offshore and Arctic Engineering, San Francisco, 2014: 33-38.

[107] LEE B E, TU J Y, FLETCHER C A J. On Numerical Modeling of Particle–Wall Impaction in Relation to Erosion Prediction: Eulerian Versus Lagrangian Method[J]. Wear, 2002, 252(3/4): 179-188.

[108] CROWE C T, SCHWARZKOPF J D, SOMMERFELD M, et al. Multiphase Flows with Droplets and Particles [M]. Boca Raton: CRC Press, 2011: 85-90.

[109] MAZUMDER Q H. Development and Validation of a Mechanistic Model to Predict Erosion in Single-phase and Multiphase Flow[M]. Oklahoma: The University of Tulsa, 2004: 67-70.

[110] MAZUMDER Q H, SHIRAZI S A, MCLAURY B S, et al. Development and Validation of a Mechanistic Model to Predict Solid Particle Erosion in Multiphase Flow[J]. Wear, 2005, 259(1/2/3/4/5/6): 203-207.

[111] QIAN S, KANAMARU S. Verification of CFD Prediction Accuracy of Particle and Droplet Induced Erosion Rate for Engineering Applications[C]//18th Asian Pacific Confederation of Chemical Engineering Congress (APCChE 2019), 2019: 19.

[112] LIU Ming-yang, LIU Hai-xiao, ZHANG Ri. Numerical Analyses of the Solid Particle Erosion in Elbows for Annular Flow[J]. Ocean Engineering, 2015, 105: 186-195.

[113] LIU Guan-lan, AYELLO F, VERA J, et al. An Exploration on the Machine Learning Approaches to Determine the Erosion Rates for Liquid Hydrocarbon Transmission Pipelines towards Safer and Cleaner Transportations[J]. Journal of Cleaner Production, 2021, 295: 126478.

[114] PANDYA D A, DENNIS B H, RUSSELL R D. A Computational Fluid Dynamics Based Artificial Neural Network Model to Predict Solid Particle Erosion[J]. Wear, 2017, 378/379: 198-210.

[115] ZHANG Z, BARKOULA N M, KARGER-KOCSIS J, et al. Artificial Neural Network Predictions on Erosive Wear of Polymers[J]. Wear, 2003, 255(1/23/4/5/6): 708-713.

[116] BOULANGER J A R, WONG C Y, ZAMBERI M S A, et al. Erosion Model Calibration with Genetic Algorithm [C]//Eleventh International Conference on CFD in the Minerals and Process Industries. Melbourne: Commonwealth Scientific and Industrial Research Organisation, 2015: 333-339.

[117] HAWKINS D M. The Problem of Overfitting[J]. Journal of Chemical Information and Computer Sciences, 2004, 44(1): 1-12.

责任编辑：彭颋

（上接第 74 页）

[65] ZHOU Z, WANG L, HE D Y, et al. Microstructure and Wear Resistance of Fe-Based Amorphous Metallic Coatings Prepared by HVOF Thermal Spraying[J]. Journal of Thermal Spray Technology, 2010, 19(6): 1287-1293.

[66] 周小东. 高耐磨铁基非晶合金涂层制备与性能研究[D]. 沈阳: 东北大学, 2015.
ZHOU Xiao-dong. Preparation and Properties of Fe-based Amorphous Metallic Coatings with High Wear Resistance[D]. Shenyang: Northeastern University, 2015.

[67] MA H R, LI J W, JIAO J, et al. Wear Resistance of Fe- Based Amorphous Coatings Prepared by AC-HVAF and HVOF[J]. Materials Science and Technology, 2017, 33(1): 65-71.

[68] FARMER J, CHOI J S, SAW C, et al. Iron-Based Amorphous Metals: High-Performance Corrosion-Resistant Material Development[J]. Metallurgical and Materials Transactions A, 2009, 40(6): 1289-1305.

[69] BLINK J, FARMER J, CHOI J, et al. Applications in the Nuclear Industry for Thermal Spray Amorphous Metal and Ceramic Coatings[J]. Metallurgical and Materials Transactions A, 2009, 40(6): 1344-1354.

[70] LI H X, LU Z C, WANG S L, et al. Fe-Based Bulk Metallic Glasses: Glass Formation, Fabrication, Properties and Applications[J]. Progress in Materials Science, 2019, 103: 235-318.

[71] KHANOLKAR G R, RAULS M B, KELLY J P, et al. Shock Wave Response of Iron-Based in Situ Metallic Glass Matrix Composites[J]. Scientific Reports, 2016, 6(1): 1-9.

[72] 聂贵茂, 黄诚, 李波, 等. 铁基非晶合金涂层制备及应用现状[J]. 表面技术, 2017, 46(11): 6-14.
NIE Gui-mao, HUANG Cheng, LI Bo, et al. Fabrication and Application Status of Fe-Based Amorphous Alloy Coatings[J]. Surface Technology, 2017, 46(11): 6-14.

[73] 皮自强, 杜开平, 郑兆然, 等. 铁基非晶合金涂层的研究进展[J]. 热喷涂技术, 2020, 12(4): 1-11.
PI Zi-qiang, DU Kai-ping, ZHENG Zhao-ran, et al. Advantages in Fe-Based Amorphous Alloy Coating Research[J]. Thermal Spray Technology, 2020, 12(4): 1-11.

[74] 黄松强, 何学敏, 周经中, 等. 热喷涂制备非晶态合金耐蚀涂层及其在电力设施防护中的应用研究进展[J]. 中国表面工程, 2021, 34(5): 92-104.
HUANG Song-qiang, HE Xue-min, ZHOU Jing-zhong, et al. Research Progress of Thermal Sprayed Amorphous Alloy Corrosion Resistant Coating and Its Application in the Protection of Power Facilities[J]. China Surface Engineering, 2021, 34(5): 92-104.

责任编辑：万长清